Am J Transl Res 2020;12(7):3842-3857
www.ajtr.org /ISSN:1943-8141/AJTR0105523

Original Article

Down-regulation of PCK2 inhibits the invasion and metastasis of laryngeal carcinoma cells

Yun Hu[1*], Kun Deng[1*], Meihong Pan[2], Shanyan Liu[2], Wenda Li[1], Jialu Huang[1], Jinwei Yao[3], Jianhong Zuo[1,2,3]

[1]Hunan Province Key Laboratory of Tumor Cellular and Molecular Pathology, Cancer Research Institute, The Laboratory of Translational Medicine, Hunan Provincial Key Laboratory of Tumour Microenvironment Responsive Drug Research, Hengyang Medical School, University of South China, Hengyang 421002, Hunan, P. R. China; [2]The Affiliated Nanhua Hospital of University of South China, Hengyang 421002, Hunan, P. R. China; [3]The Third Affiliated Hospital of University of South China, Hengyang 421900, Hunan, P. R. China. [*]Equal contributors.

Received November 26, 2019; Accepted May 31, 2020; Epub July 15, 2020; Published July 30, 2020

Abstract: Laryngeal carcinoma is one of the common malignancies of head and neck. However, the pathogenesis of laryngeal cancer has been not completely clear. To identify the effects of hypoxia on the invasion, metastasis, and metabolism of laryngeal carcinoma, iTRAQ-labeling-with-LC-MS/MS analysis was performed to identify differentially expressed proteins of the SCC10A cells under hypoxia and normoxia, while metabolites were examined by metabolic profiling. 155 proteins and 180 metabolites were identified and the PCK2 protein was selected for validation by Western Blotting. Immunohistochemistry (IHC) was performed to analyze the expression of PCK2 in formalin-fixed paraffin-embedded (FFPE) tissue sections, including laryngeal squamous cell carcinoma tissues from various stages. Collectively, we report that down-regulation of PCK2 inhibits the invasion, migration, and proliferation of laryngeal cancer under hypoxia and down-regulation of PCK2 may be used as a new strategy for laryngeal cancer therapy.

Keywords: Laryngeal cancer, hypoxia, PCK2, invasion, metastasis

Introduction

Laryngeal cancer is one of the frequently occurring malignancies among head and neck squamous cell carcinoma, which is common among males [1]. The incidence of laryngeal cancer has been increasing in the recent years [2]. The majority of laryngeal cancer is laryngeal squamous cell carcinoma [3, 4] of which genetic and environmental factors are considered as the main cause of laryngeal cancer [5]. Although great progress has been made in the diagnosis and treatment of laryngeal cancer, 30-40% patients still die of tumor metastasis [6]. Hypoxia activates transcription factors that regulate cell survival, angiogenesis, and metastasis to promote tumor progression [7, 8]. Therefore, it is highly important to understand the role of hypoxia in laryngeal cancer.

Compared with normal tissue, the unlimited proliferation of tumor cells would lead to increased oxygen consumption, for the reason that most solid tumors have hypoxia regions [9]. Thus, hypoxia is a hallmark of solid tumors [10], which promotes tumor cell invasion and metastasis [11]. Under hypoxia, glycolysis is upregulated [12] and lactate level increases in cells [13]. This glucose metabolism is an important characteristics of solid tumors that mainly initiated from GLUT-1. Aerobic glycolysis, also termed the "Warburg Effect", is significantly accelerated in tumors [14], and glucose concentration is decreased, resulting in hypoglycemia in the tumor cells [15]. Tumor cells with limited glucose intake rely on mitochondrial oxidative phosphorylation to maintain cell proliferation [14].

To investigate the possible effects of hypoxia on laryngeal cancer, proteomic profiling was performed in this study to identify differentially expressed proteins under hypoxia and normoxia in laryngeal cancer SCC10A cells. A differentially expressed protein PCK2 was selected for further validation. Furthermore, the present study aims to dissect the effects of PCK2 in invasion, migration, and proliferation of laryngeal cancer, the relationship between PCK2 and cancer cell metabolism, and the associa-

tion between PCK2 expression and clinical characteristics of laryngeal cancer patients.

Materials and methods

Reagents and antibodies

The following antibodies were used: GLUT1 (Proteintech, China, 21829-1-AP), PCK2 (Proteintech, China, 14892-1-AP), and β-actin (Biosharp, China, BL005B). Anti-mouse and anti-rabbit secondary antibodies, conjugated to horseradish peroxidase for Western blotting, were obtained from Licor.

Cell culture

Human laryngeal cancer cell line, SCC10A, was maintained in Dulbecco's modified Eagle's medium (DMEM, Gibco; Thermo Fisher Scientic, Inc), supplemented with 10% fetal bovine serum (Gibco; Thermo Fisher Scientic, Inc), 100 U/ml penicillin and 100 μg/ml streptomycin (Gibco; Thermo Fisher Scientic, Inc). Cells were cultured in an incubator at 37°C with 5% CO_2 (Eppendorf, GER). To mimic hypoxia, cells were cultured in cobalt chloride hexahedron ($CoCl_2{\cdot}6H_2O$, Aladdin) [16, 17], which was dissolved in DMEM as a 2,000x concentrate and was diluted to 200 μM for experiments [18]. The cells were cultured for 12 h with $CoCl_2$ before cells were collected.

TMT/iTRAQ labeling

After cell harvest, four volumes of lysis buffer (8M urea, 1% protease inhibitor, 3 μM TSA, 50 mM NAM and 2 mM EDTA) were added to the cells and the cells were sonicated. Cell debris were removed by centrifugation at 12,000 g at 4°C for 10 min. Then, the supernatant was transferred to a new centrifuge tube. The protein concentration was determined with a BCA kit (Bio-Rad Laboratories, Hercules, CA) according to the manufacturer's instructions. The protein solution was added to 5 mM dithiothreitol for 30 min at 56°C and alkylated with 11 mM iodoacetamide for 15 min at room temperature in darkness. The protein samples were then diluted by adding 100 mM TEAB to urea concentration less than 2M. Finally, trypsin was added at 1:50 trypsin-to-protein mass ratio for the first digestion overnight and 1:100 trypsin-to-protein mass ratio for a second 4 h-digestion.

After trypsin digestion, peptides were desalted by Strata X C18 SPE column (Phenomenex) and vacuum-dried. Peptides were reconstituted in 0.5 M TEAB and processed according to the manufacturer' s protocol for TMT kit/iTRAQ kit. Briefly, one unit of TMT/iTRAQ reagent was thawed and reconstituted in acetonitrile. The peptide mixtures were then incubated for 2 h at room temperature and pooled, desalted and dried by vacuum centrifugation.

LC-MS/MS analysis

The tryptic peptides were dissolved in 0.1% formic acid (solvent A), directly loaded onto a home-made reversed-phase analytical column (15-cm length, 75 μm inner diameter). The gradient was comprised of an increase from 6% to 23% solvent B (0.1% formic acid in 98% acetonitrile) over 26 min, 23% to 35% in 8 min and climbing to 80% in 3 min then holding at 80% for the last 3 min, all at a constant flow rate of 0.4 μL/min on an EASY-nLC 1000 UPLC system.

The peptides were subjected to NSI source followed by tandem mass spectrometry (MS/MS) in Q Exactive™ Plus (Thermo) coupled online to the UPLC. The electrospray voltage applied was 2.0 kV. The m/z scan range was 350 to 1800 for full scan, and intact peptides were detected in the Orbitrap at a resolution of 70,000. Peptides were then selected for MS/MS using NCE setting as 28 and the fragments were detected in the Orbitrap at a resolution of 17,500. A data-dependent procedure that alternated between one MS scan followed by 20 MS/MS scans with 15.0s dynamic exclusion. Automatic gain control (AGC) was set at 5E4. Fixed first mass was set as 100 m/z.

Bioinformatic analysis

Gene Ontology (GO) annotation of the proteome was derived from the UniProt-GOA database (www.http://www.ebi.ac.uk/GOA/). The InterProScan software was used to annotate protein's GO functional based on protein sequence alignment method for some proteins that were not annotated by UniProt-GOA database. KEGG online service tools KAAS (https://www.genome.jp/tools/kaas/) was used to annotate proteins' KEGG database description and KEGG online service tools KEGG mapper was used to map the annotation results on the KEGG path-

way database. The GO and the KEGG Pathway with a corrected $P < 0.05$ are considered significant. Hierarchical clustering was performed on the differentially expressed proteins in laryngeal cancer that was visualized by a heatmap, which used the heatmap.2 function from the plots R-package.

Cells sample preparation and analysis by gas chromatography-time-of-flight mass spectrometry (GC-TOFMS)

The sample preparation procedure was previously described by Qiu et al [19] and Wang et al [20]. Briefly, frozen cell samples were harvested and stored in an Eppendorf SafeLock microcentrifuge tube, mixed with 25 mg of pre-chilled zironium oxide beads and 10 μL of internal standard. Each aliquot of 50 μL of 50% prechilled methanol was added for automated homogenization (BB24, Next Advance, Inc., Averill Park, NY, USA). After centrifugation at 14,000 g and 4°C for 20 min (Microfuge 20R, Beckman Coulter, Inc, Indianapolis, IN, USA), the supernatant was carefully transferred to an autosampler vial (Agilent Technologies, Foster City, CA, USA). Each aliquot of 175 μL of prechilled methanol/chloroform (v/v = 3/1) was added to the residue for the second extraction. After centrifugation at 14,000 g and 4°C for 20 min, each 200 μL of the supernatant was carefully transferred to an autosampler vial. The remaining supernatant from each sample was pooled to make quality control samples. All the samples in autosampler vials were evaporated briefly to remove chloroform using a CentriVap vacuum concentrator (Labconco, Kansas City, MO, USA), and further lyophilized with a FreeZone freeze dryer equipped with a stopping tray dryer (Labconco, Kansas City, MO, USA).

The sample dericatization and injection were performed by a robotic multipurpose sample MPS2 with dual heads (Gerstel, Muehlheim, Germany). Briefly, the dried sample was derivatized with 50 μL of methoxyamine (20 mg/mL in pyridine) at 30°C for 2 h, followed by the addition of 50 μL of MSTFA (1% TMCS) containing FAMEs as retention indices at 37.5°C for another 1 h using the sample preparation head. In parallel, the derivatized samples were injected with sample injection head after dericatization.

Each 1 μL aliquot of the derivatized solution was injected in splitless mode into an Agilent 7890N gas chromatography and a Gerstel multipurpose sample MPS2 with dual heads, which were coupled with a time-of-flight mass spectrometry (GC-TOFMS) system (Pegasus HT, Leco Corporation, St. Joseph, MO, USA). The laryngeal cancer and control samples were run in the order of "control-LC-control", alternately, to minimize systematic analytical deviations. A Rxi-5 ms capillary column (30 m × 250 μm i.d., 0.25 μm film thickness; Restek corporation, Bellefonnte, PA, USA) was used for separation. Helium was used as the carrier gas at a constant flow rate of 1.0 mL/min. The temperature of injection and transfer interface were both set to 270°C. The GC temperature programming was set to 2 min isothermal heating at 80°C, followed by 12°C/min oven temperature ramps to 300°C, 4.5 min maintenance at 300°C, 40°C/min to 320°C, and a final 1 min maintenance at 320°C. Electron impact ionization (70 eV) in the full scan mode (m/z 50-500) was used, with an acquisition rate of 25 spectra/s in the TOFMS setting.

GC-TOFMS data analysis

The raw data generated by GC were processed using Xplore for automated baseline denosing and smoothing, peak picking and deconvultion, creating reference database from the pooled QC samples, metabolite signal alignment, missing value correvtion and imputation, and QC correction. The resulting data were normalized to internal standards and the sum of cell samples before statistical analysis. Principal component analysis (PCA) and orthogonal partial least squares discriminant analysis (OPLS-DA) were performed with statistical analysis software packages in R studio (http://cran.r-project.org/). The default 7-fold cross-validation was applied to guard against overfitting. The variable importance in the projection (VIP) values (VIP > 1.0) is considered to be differentiating variables [21]. T-test is used to determine whether the two sets of data are significantly different or not. The *p*-value gives the amount evidence that the two sets of data are different through the t-statistic. A conservative nonparametric method, U-test, was also used to test the significance of the two sets of data. Fold change was calculated by the ratio of means or medians between the pairwise comparisons

using T-test or U-test, respectively. The calculated fold change of 1.5 or *p*-value of 0.05 is chosen for statistical significance. The V-plot that integrated the fold change and *p*-values was used for depiction the (of the) significantly different metabolites.

Western blotting

Cultured cells were harvested in lysis buffer, and protein concentration was determined by a BCA protein assay kit. Proteins separated by SDS-PAGE, and transferred to PVDF membranes. Blots were blocked with 5% fat-free milk for 1 h at temperature and incubated with primary antibodies overnight at 4°C. The membranes were incubated with secondary antibody (1:1500) and the signal was visualized with ECL detection reagent. β-actin was simultaneously detected using rabbit anti-β-actin antibody as a loading control.

Transfection

For RNA interference analysis, small interfering RNA (siRNA) targeting human PCK2 (Ribobio, China) were (was) delivered into SCC10A cells using Lipofectamine 2000 reagent (Thermo Fisher Scientific) according to the manufacturer's protocol. In addition, the non-targeting siRNA pool (Ribobio, China) was used at the same concentration of 100 nM as a control for the RNA interference assays. Four hours following transfection, the medium was replaced with DMEM containing 10% FBS and the cells were cultured for 44 hours. At the end of the transfection, cells were subjected to migration and invasion assays as described below and protein expression was determined by Western Blotting analysis.

Migration and invasion assays

In the transwell migration assay, as previously described [22, 23], the upper chamber of the 24-well transwell with 8μm pore size (Corning Incorporated), 1×10^5 cells in serum-free DMEM were added. 500 μl DMEM was added in the bottom chambers and analyzed after 6 h at 37°C. The insert was fixed with 4% paraformaldehyde for 15 min and stained with 0.1% crystal violet for 30 min at 37°C. Non-migrating cells retained on the upper side were removed by wiping with a cotton swab. Cells that had migrated through the filter were counted and averaged from 3 randomly selected microscopic fields (20 × objective).

In vitro invasion assays, the upper chambers were precoated with Matrigel (BD) and maintained at 37°C and 5% CO_2 for 1 h. Cells (1×10^5) in 200 μL of serum-free DMEM were added on the top of the transwell. Serum-free medium was then added to the lower chamber and incubated for 24 h at 37°C. Cells were fixed and stained with 0.1% crystal violet, Matrigel and associated cells were removed with a cotton swab. Cells that had penetrated the Matrigel and had reached the underside of the filter membrane were then counted and averaged from 3 randomly selected microscopic fields (20 × objective).

MTT assay

The proliferation capacity of three groups cells (control, empty vector and PCK2 transfected) was measured by 3-(4,5-dimethyl-2-thiazolyl)-2,5-diphenyltetrazolium bromide (MTT) assay. Cells (approximately 5×10^3) were grew into 96-well plates for 24 h, 48 h, and 72 h. Then 20 μL MTT (5 mg/mL) was added to the cells for 4h at 37°C. Before measured, 150 μL DMSO was added for 20 min at room temperature on the horizontal shaker. The optical density was measured with a microplate reader (Bio-Rad) at a wavelength of 490 nm. The inhibition rate (IR) of transfected SCC10A cells was calculated as follows: IR = (1-OD treated/OD untreated) × 100%.

ATP measurement

The content of ATP was assayed using the ATP Assay Kit (Jiancheng Bio Ins, China) according to manufacturers' manual. Briefly, the cells were digested, centrifuged, and the supernatant was discarded. 300-500 μL distilled water was added before the homogenate was centrifuged in hot water bath at 90-100°C, and heated in water bath for 10 min, then extracted and mixed for 1 min. 30 μL 1 mol/L standard solution was added to the blank tube and the standard tube, 30 μL sample solution was added to the measuring tube and the control tube, the working solution was added to the 4 tubes in a 37°C water bath for 30 min. The mixture was centrifuged at 4000 rpm for 5 min after 50 μL

of precipitant was added. 300 μL supernatant was taken for measurement each tube. 500 μL coloring solution and 500 μL terminator was added in sequence, mixed and stand for 5 minutes at room temperature each time. The optical density was measured with a microplate reader (Mapada) at a wavelength of 636 nm, repeated for three times. The ATP concentration in the cells was calculated as follows: ATP concentration (μmol/gprot) = (OD measure - OD control)/(OD standard-OD blank) × standard concentration (1×10^3 μmol/L) × sample dilution factor before determination/sample protein concentration.

Glucose measurement

The glucose uptake was measured using a Glucose Assay Kit (Solarbio). The assay was performed according to manufacturers' manual. Briefly, two groups of cells (cells in hypoxia and cells in normoxia) were digested, centrifuged, and the supernatant was discarded. 1 mL distilled water was added to 5×10^5 cells. Cells were ultrasonically disrupted, and kept in a water bath for 10 minutes at 95°C. After cooling, cells were centrifuged at 8000 rpm for 10 min at 25°C and the supernatant was collected. Working reaction mixture was prepared by mixing reagent two and reagent three at 1:1. 20 μL distilled water, 20 μL reagent one and 20 μL sample were added into blank tube, standard tube, and measuring tube respectively. The reactions were initiated by the addition of 180 μL of working reaction mixture. The optical density was measured with a microplate reader (Mapada) at a wavelength of 505 nm after incubation at 37°C for 15 minutes. The glucose concentration in the cells was calculated as follows: glucose concentration (μmol/10^4 cell) = 0.001 × (OD measure - OD blank)/(OD standard - OD blank).

Tissue samples

Fifty-two laryngeal cancer tissue samples were collected from patients in the Second Affiliated Hospital of University of South China from May 2012 to December 2013. The patients have not received any treatment before surgery. Fifty-two normal tissue samples were obtained from the Third Affiliated Hospital of University of South China as controls. Tumor stage was defined according to the sixth edition of Laryngeal Cancer Staging International Standards that revised by UICC in 2002. The informed consent to the study was signed by all the patients, which was approved by the University of South China Ethical Committee.

Immunohistochemistry

Immunohistochemistry (IHC) analysis of GLUT-1 and PCK2 was carried out in FFPE tissue sections using the standard immunohistochemical technique as we previously reported [24].

Statistical analysis

Statistical analysis was performed by using SPSS 17.0. Data were processed by the GraphPad Prism 5.0 software, and expressed as the mean ± standard deviation. ANOVA was used in multiple comparisons, and student's t-test was performed between two groups. The Chi-square test was used to analyze the relationship between GLUT-1 and PCK2 expression and clinical pathological characteristics in laryngeal cancer. The relationship between GLUT-1 and PCK2 protein was analyzed by Spearman correlation test. $P < 0.05$ was considered as significant.

Results

Identification of differentially expressed proteins of laryngeal cancer under hypoxia

To identify differentially expressed proteins in the laryngeal cancer cells under hypoxia, proteomic profiles of SCC10A cells cultured with or without $CoCl_2$ was compared using iTRAQ labeling and LC-MS/MS. $CoCl_2$ treatment is well-known to be able to induce cellular hypoxic responses and thus, was used to mimic hypoxia [25]. Proteins that consistently showed an average fold change ≥ 1.5 or ≤ 0.667 in the triplicate experiments between these two conditions were considered as differentially expressed (t test, $P < 0.05$). As a result, 155 proteins were identified (Supplementary Table 1).

To understand the biological significance of these differentially expressed proteins of laryngeal cancer with or without $CoCl_2$ treatment, GO and KEGG Pathway analysis was performed. Both GO and KEGG analysis results were consistent, identifying similar pathways that were changed when cells were cultured with $CoCl_2$,

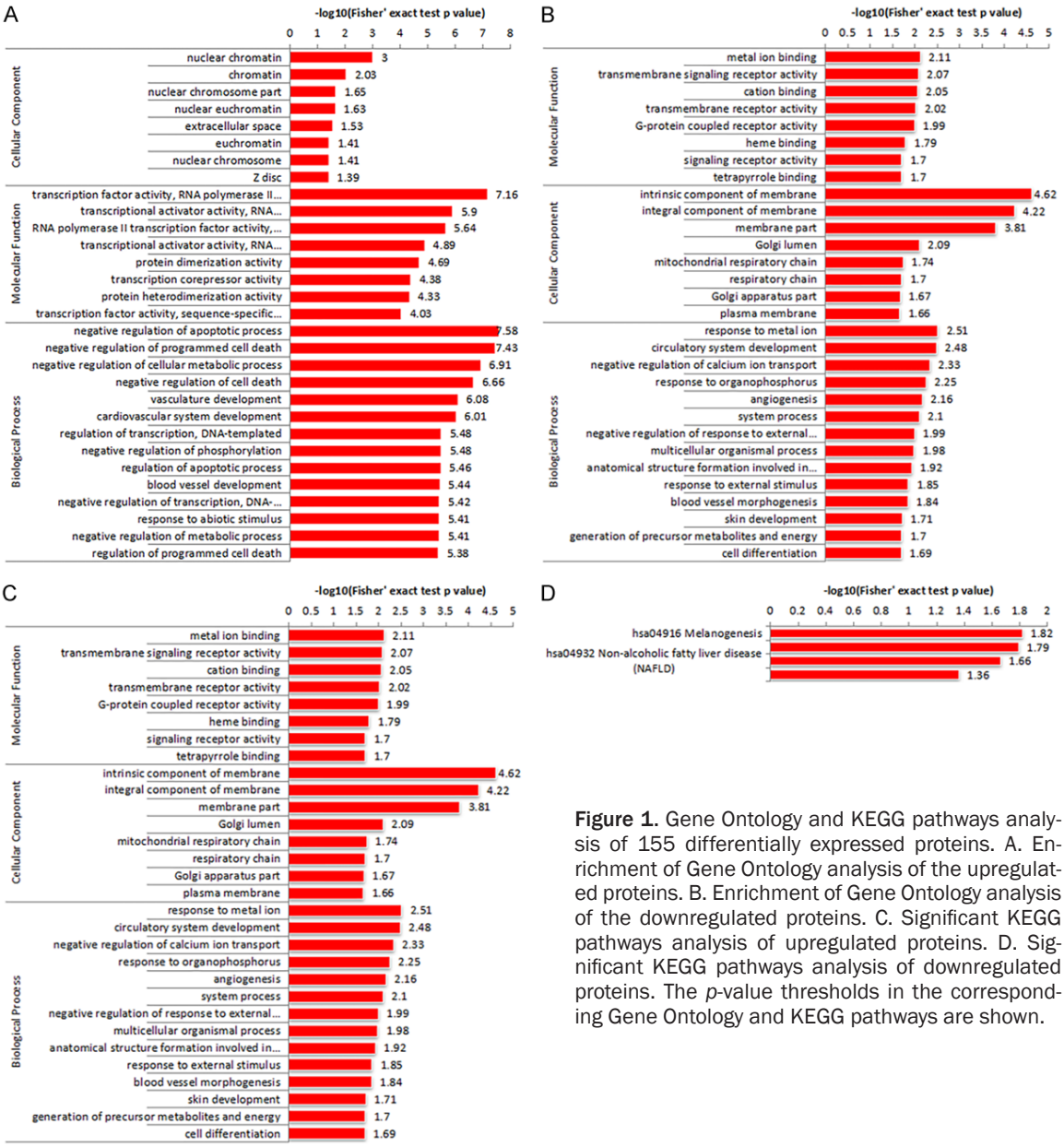

Figure 1. Gene Ontology and KEGG pathways analysis of 155 differentially expressed proteins. A. Enrichment of Gene Ontology analysis of the upregulated proteins. B. Enrichment of Gene Ontology analysis of the downregulated proteins. C. Significant KEGG pathways analysis of upregulated proteins. D. Significant KEGG pathways analysis of downregulated proteins. The *p*-value thresholds in the corresponding Gene Ontology and KEGG pathways are shown.

especially the MAPK, AMPK, and metabolic pathways (**Figure 1**). Hierarchical clustering analysis was performed on significantly up-regulated or down-regulated proteins based on GO enrichment and KEGG pathway analysis. The results indicated that proteins with functions on negative regulation of cell death, gene transcription, MAPK activity, and metabolism were enriched in samples treated with $CoCl_2$ and proteins with functions on oxidative phosphorylation and membranes were enriched in samples without $CoCl_2$ treatment (Supplementary Figure 1). These results are consistent with what we have known for biological changes cells usually make under hypoxic stress, lending strong support to the strategy of our study.

Metabolomics analysis of laryngeal cancer in hypoxia

In order to further understand metabolic changes that cells make under hypoxia, we compared metabolite profiles of the SCC10A cells cultured with or without $CoCl_2$ using GC-TOFMS. The OPLSDA model was applied to the data analysis and the scores plot showed two distinct clusters (with or without $CoCl_2$) apart from each other (**Figure 2A**), demonstrating a distinct me-

A

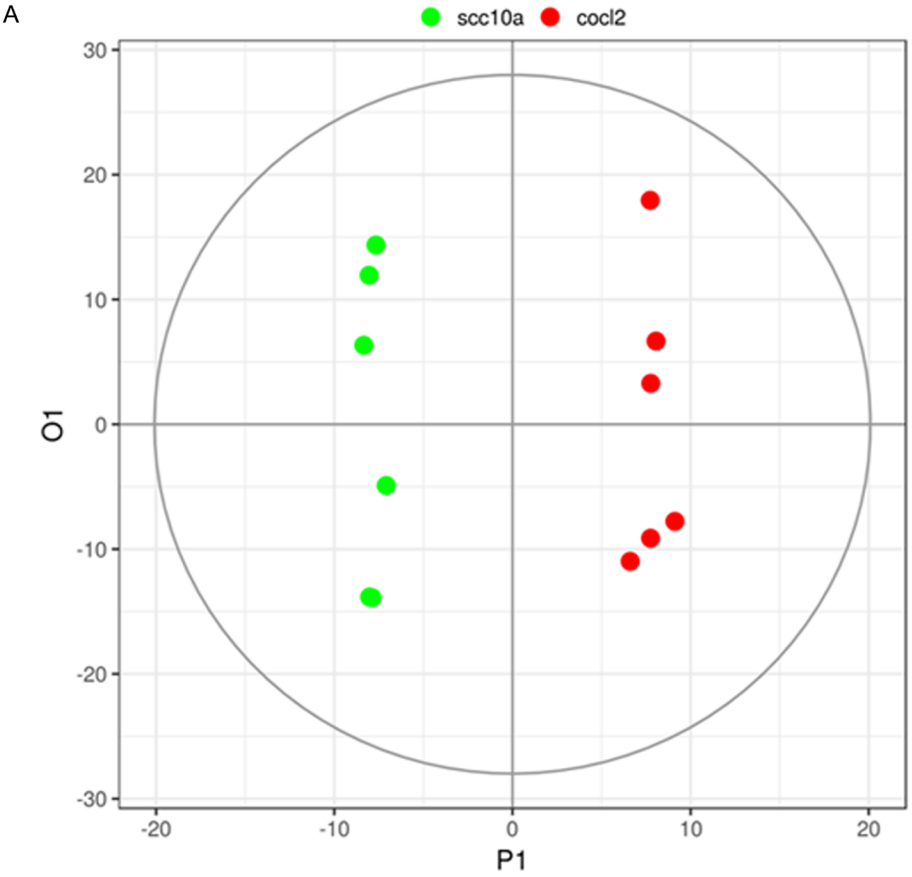
scc10a
cocl2
O1
P1
30
20
10
0
-10
-20
-30
-20
-10
0
10
20

B

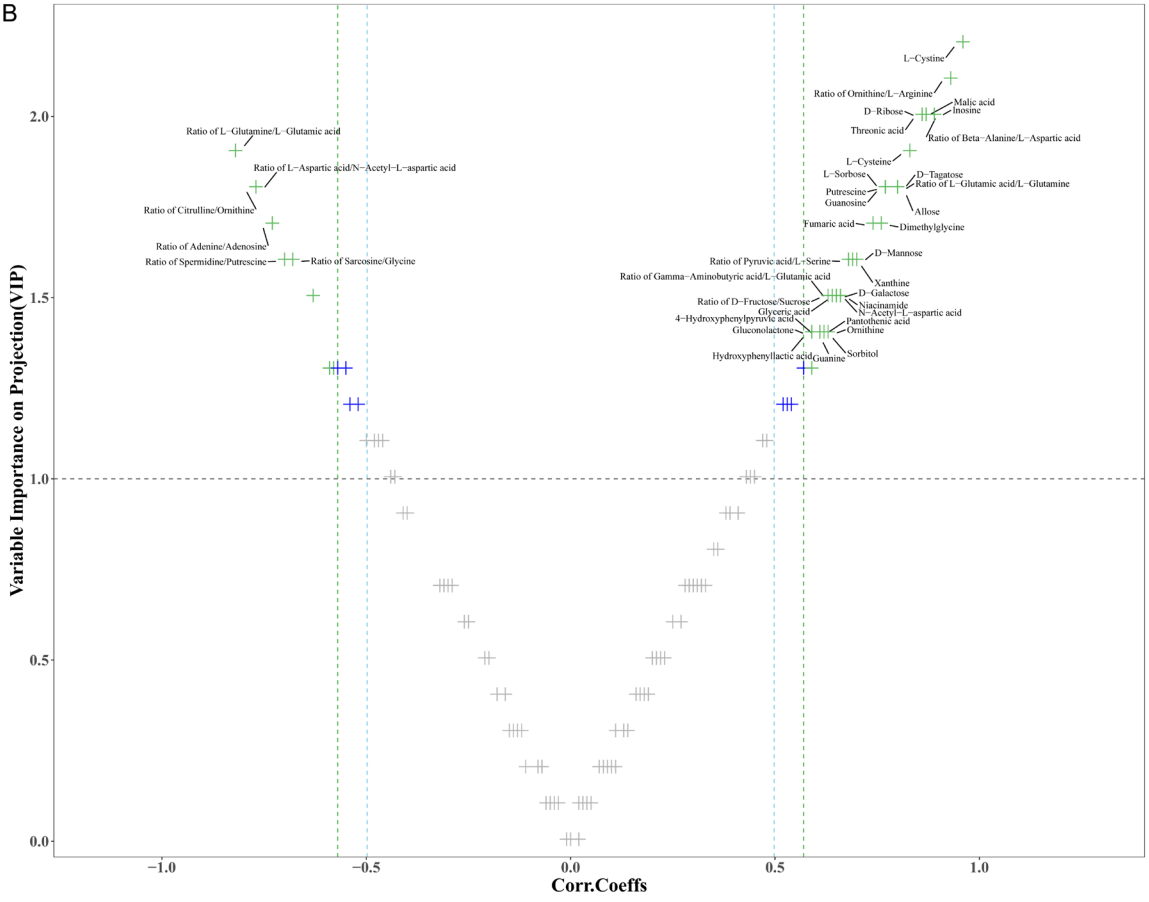
Variable Importance on Projection(VIP)
Corr.Coeffs
2.0
1.5
1.0
0.5
0.0
−1.0
−0.5
0.0
0.5
1.0
Ratio of L−Glutamine/L−Glutamic acid
Ratio of L−Aspartic acid/N−Acetyl−L−aspartic acid
Ratio of Citrulline/Ornithine
Ratio of Adenine/Adenosine
Ratio of Spermidine/Putrescine
Ratio of Sarcosine/Glycine
L−Cystine
Ratio of Ornithine/L−Arginine
D−Ribose
Malic acid
Inosine
Threonic acid
Ratio of Beta−Alanine/L−Aspartic acid
L−Cysteine
L−Sorbose
D−Tagatose
Putrescine
Ratio of L−Glutamic acid/L−Glutamine
Guanosine
Allose
Fumaric acid
Dimethylglycine
Ratio of Pyruvic acid/L−Serine
D−Mannose
Ratio of Gamma−Aminobutyric acid/L−Glutamic acid
Xanthine
D−Galactose
Ratio of D−Fructose/Sucrose
Niacinamide
Glyceric acid
N−Acetyl−L−aspartic acid
4−Hydroxyphenylpyruvic acid
Pantothenic acid
Gluconolactone
Ornithine
Hydroxyphenyllactic acid
Guanine
Sorbitol

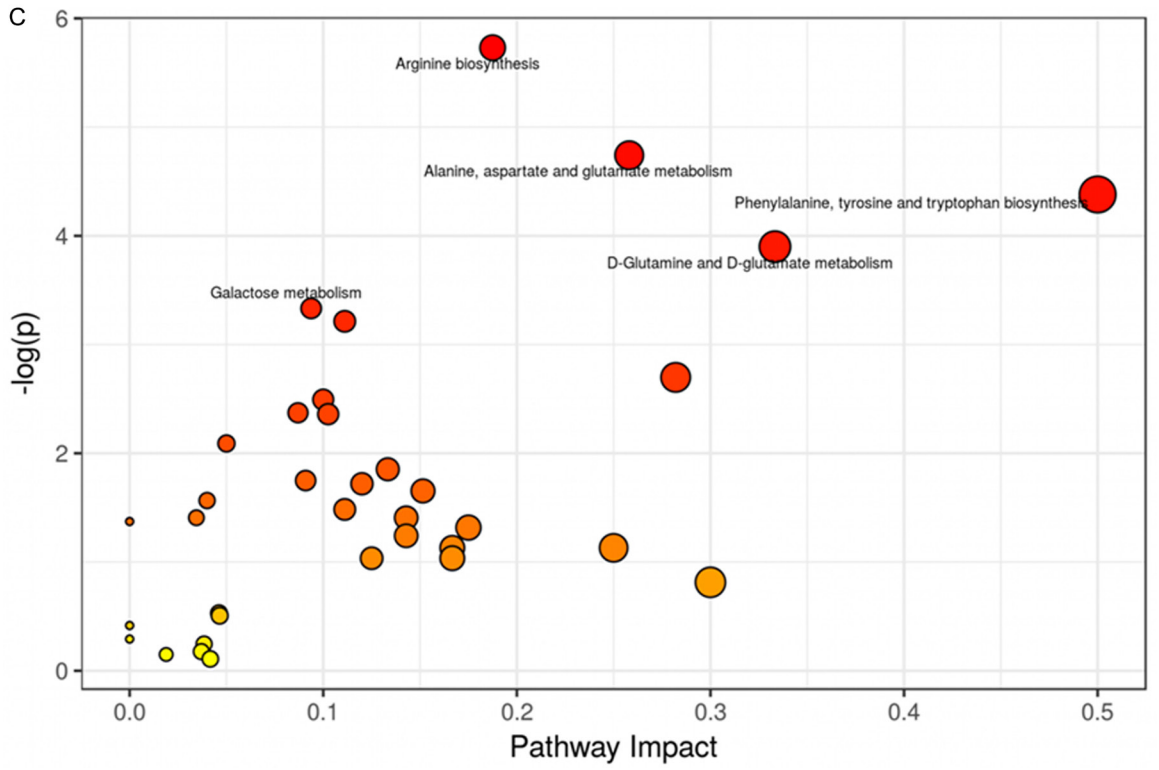

Figure 2. Identification of differentially produced metabolites from the SCC10A cells cultured with or without $CoCl_2$ by GC-TOFMS. A. OPLS-DA scores plots of differentially expressed metabolites in the SCC10A cells culture without $CoCl_2$ (representing normoxia) or with $CoCl_2$ (representing hypoxia). B. V-plots of differentially produced metabolites in the SCC10A cells cultured with or without $CoCl_2$. C. Summaries of the Metabolic Pathway Enrichment Analysis results.

tabolite profiles between these two groups of cells. A V-plot model was used to select metabolites that were differentially produced in cells with or without $CoCl_2$ (**Figure 2B**). The metabolic pathway enrichment analysis results are summarized in **Table 1** and **Figure 2C**. The top-ranked metabolites from the univariate statistical analysis are illustrated in Supplementary Figure 2.

The biological functions of PCK2 in laryngeal cancer

Among these differentially expressed proteins, PCK2 showed significant changes at the presence of $CoCl_2$ (Supplementary Figure 3). Western blotting was used to validate PCK2 proteomic profiling results. Indeed, expression of PCK2 was increased in SCC10A cells when cultured with $CoCl_2$ (**Figure 3A**).

To investigate the role of PCK2 function, invasion, migration, and proliferation of SCC10A cells were examined when PCK2 is down-regulated by an siRNA (**Figure 3B**). Invasion and migration of SCC10A cells was markedly decreased after PCK2 was knocked down (**Figure 3C-F**). MTT assay was performed to examine the effect of PCK2 on SCC10A cell proliferation. SCC10A cell proliferation was markedly decreased following PCK2 knockdown compared to that of control cells (**Table 2**). Together, these results indicated that down-regulation of PCK2 decreased the invasion, migration and proliferation of laryngeal cancer SCC10A cells.

Since metabolic pathway was significantly altered in the SCC10A cells treated with $CoCl_2$, we examined whether cellular glucose uptake and ATP generation reflect these changes. As expected, glucose uptake and ATP content of SCC10A cells increased when cultured with $CoCl_2$ (**Figure 4A**, **4B**). Conversely, the glucose content and ATP generation in the SCC10A cells decreased when PCK2 is knocked down (**Figure 4C**, **4D**), suggesting that PCK2 plays a role in glycolysis in the SCC10A cells.

Table 1. Differentially regulated metabolic pathways when the SCC10A cells were cultured with $CoCl_2$

Pathway Name	P. hyper	Impact	Up	Down
Arginine biosynthesis	3.25e-03	0.19	Fumaric acid; Oxoglutaric acid; Ornithine	L-Glutamine
Alanine, aspartate and glutamate metabolism	8.73e-03	0.26	Gamma-Aminobutyric acid; Fumaric acid; Oxoglutaric acid; NAcetyl-L-aspartic acid	L-Glutamine
Phenylalanine, tyrosine and tryptophan biosynthesis	1.25e-02	0.50	4-Hydroxyphenylpyruvic acid	L-Phenylalanine
D-Glutamine and D-glutamate metabolism	2.02e-02	0.33	Oxoglutaric acid	L-Glutamine
Galactose metabolism	3.57e-02	0.09	D-Galactose; D-Mannose; Alpha-Lactose; Sorbitol	
Glutathione metabolism	4.02e-02	0.11	Glycine; Ornithine; L-Cysteine; Putrescine	
Glycine, serine and threonine metabolism	0.067	0.28	Dimethylglycine; Glycine; Glyceric acid; L-Cysteine	
Pentose phosphate pathway	0.083	0.10	Glyceric acid; Gluconolactone; D-Ribose	
Purine metabolism	0.093	0.09	Guanine; Guanosine; Inosine; Xanthine	Adenine; L-Glutamine
Amino sugar and nucleotide sugar metabolism	0.094	0.10	D-Galactose; D-Mannose; D-Fructose	Fructose 6-phosphate

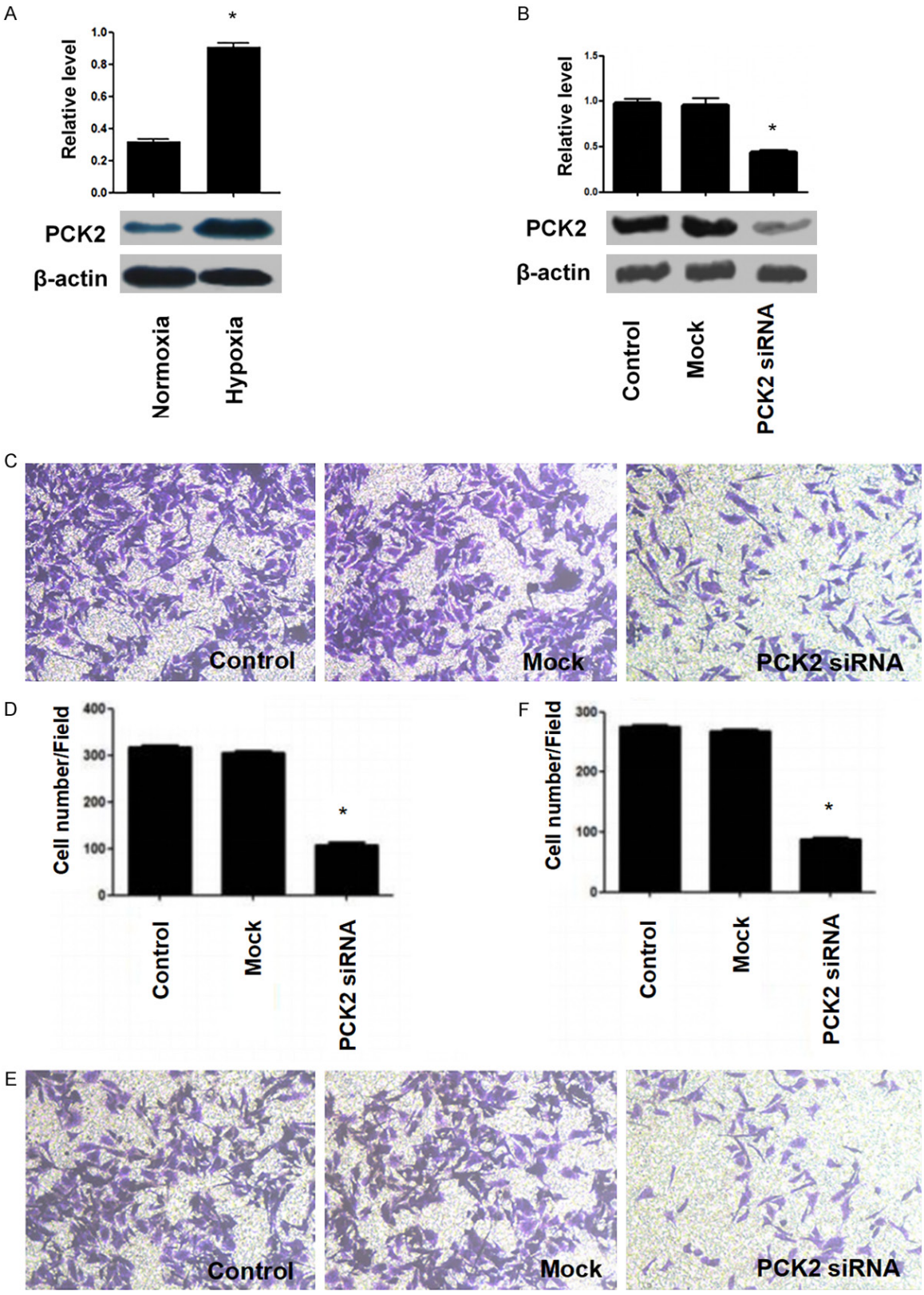

Figure 3. Characterization of PCK2 function. A. PCK2 was induced when the SCC10A cells were cultured with $CoCl_2$. B. siRNA effectively downregulates PCK2 expression. C. Representative images of cell invasion assay following PCK2 knockdown by siRNAs. D. Quantification of the number of cells in the invasion assay that migrated through the transwell membranes by counting at least three random microscopic fields. E. Representative images of cell migra-

tion assay following PCK2 knockdown by siRNAs. F. Quantification of the number of cells in the migration assay that migrated through the transwell membranes by counting at least three random microscopic fields. Error bars indicate standard deviation. Student's t-test was performed for statistical analysis, $^{*}P < 0.05$.

Table 2. OD value and IR of the SCC10A cells following PCK2 knockdown ($\bar{x} \pm s$, n = 3)

Time (h)	Control	Empty vector	PCK2-transfected	IR (%)
24	0.724±0.141	0.752±0.123	0.611±0.018	23.08
48	1.091±0.213	1.066±0.218	0.684±0.024	35.83
72	1.254±0.341	1.239±0.154	0.772±0.025	36.07

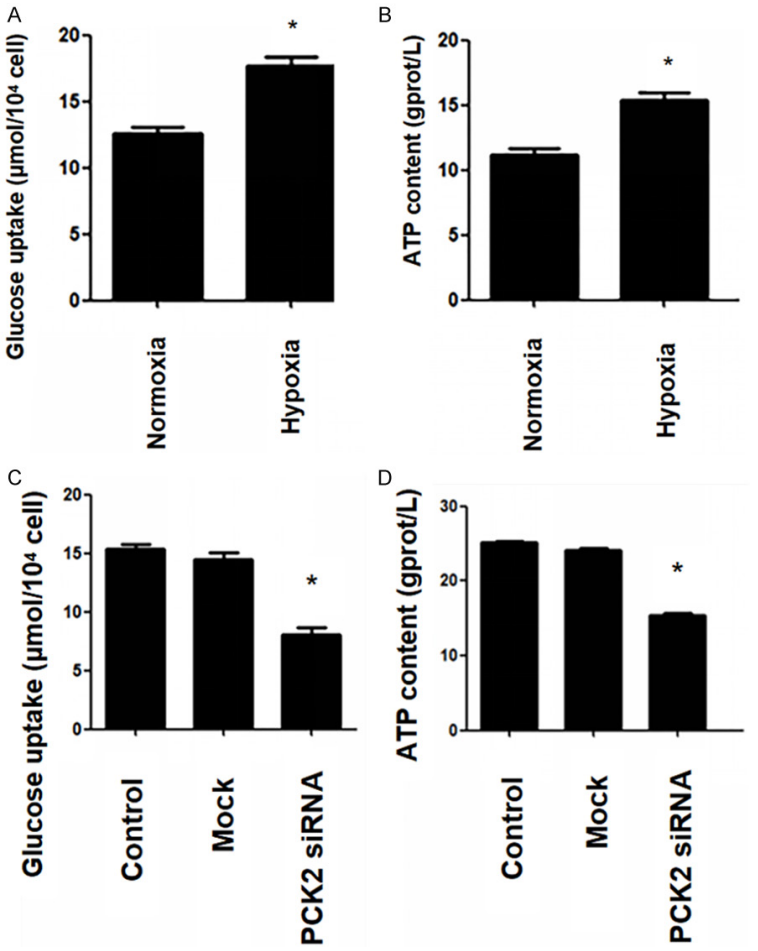

Figure 4. PCK2 regulates SCC10A cell metabolism. A. Glucose uptake of the SCC10A cells when cultured with or without $CoCl_2$. B. ATP content in the SCC10A cells when cultured with or without $CoCl_2$. C. Glucose uptake changes in the SCC10A cells when PCK2 is down-regulated by siRNAs. D. Cellular ATP content changes in SCC10A cells when PCK2 is down-regulated by siRNAs. Error bars indicate standard deviation. Student's t-test was performed for statistical analysis, $^{*}P < 0.05$.

GLUT-1 and PCK2 are highly expressed in laryngeal cancer

To determine whether there is a direct link between tumor hypoxia and PCK2, the expression of GLUT-1 (a well-known surrogate marker for tumor hypoxia) and PCK2 was examined by IHC in normal laryngeal squamous epithelial tissues and laryngeal squamous cell carcinoma tissues. Interestingly, expression of both GLUT-1 and PCK2 is low in normal tissues but much higher in laryngeal cancer tissues ($P < 0.05$) (**Figure 5**). Specifically, 11.53% (6/52) and 9.61% (5/52) of normal laryngeal squamous epithelial tissues were stained positive for GLUT-1 and PCK2, respectively. However, 84.61% (44/52) and 82.69% (43/52) of laryngeal squamous cell carcinoma tissues were stained positive for GLUT-1 and PCK2, respectively. Thus, a significant difference of expression was detected between normal tissues and carcinoma tissues for both proteins ($P < 0.05$) (**Table 3**).

Expression of GLUT-1 and PCK2 in laryngeal cancer tissue is not related to sex, age, tissue type, and anatomical type of the patients ($P > 0.05$), but it is associated with clinical stage and lymph node metastasis ($P < 0.05$) (**Table 4**). In addition, there is a positive correlation between the expression of GLUT-1 and PCK2 in laryngeal squamous cell carcinoma by Spearman correlation ($P < 0.05$) (**Table 5**).

Discussion

Laryngeal cancer is one of most common malignancies of head and neck. The majority of laryngeal cancer patients are middle-aged or old male [26]. In recent years, the number of female patients has been increasing [1].

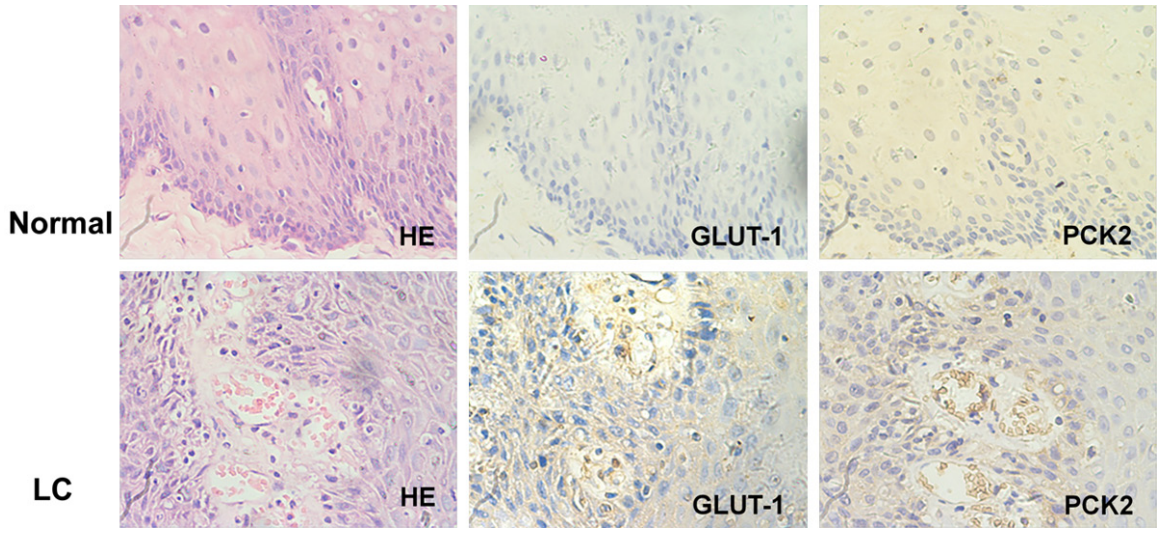

Figure 5. Immunohistochemistry analysis of GLUT-1 and PCK2 expression in normal laryngeal squamous epithelial tissues (Normal) and laryngeal squamous carcinoma tissues (LC). Original magnification, 10 × 40.

Table 3. Expression of GLUT-1 and PCK2 in normal laryngeal squamous epithelial tissues and laryngeal squamous cell carcinoma tissues

Group	*n*	GLUT-1			PCK2		
		+	-	*P*	+	-	*P*
Normal	52	6	46	< 0.05	5	47	< 0.05
Carcinoma	52	44	8		43	9	

Therefore, it is important to diagnose and treat laryngeal cancer at early stages [27, 28]. Currently, the combination of surgery and radiotherapy is the main treatment option for most laryngeal cancer patients [29]. Although the multidisciplinary treatment model has been applied in the treatment of laryngeal cancer, the effect remains far from satisfactory. Previous studies have indicated that hypoxia promotes invasion and metastasis of tumor cells, however, the role of hypoxia in laryngeal cancer remains unknown.

Our study identified 155 differentially expressed proteins and 39 differentially generated metabolites from laryngeal cancer SCC10A cells cultured with $CoCl_2$, a molecule that mimics many aspects of hypoxia effects on cells. Among the metabolites, D-Allose is a rare sugar which showed promising anti-proliferative and pro-apoptotic activity in cancer cell [30]. Clear cell renal cell carcinoma, a unique cancer type with constitutive activation of the HIF-1α pathway due to frequent mutation of the von Hippel Lindau gene (*VHL*), is metabolically distinct from clear cell papillary renal cell carcinoma, primarily by high-level metabolites from the sorbitol metabolic pathway [31]. Sorbitol induces the expression of HIF-1α protein in three renal carcinoma cell lines, a new mechanism of HIF pathway activation in clear cell papillary renal cell carcinoma [31]. Many other identified metabolites have distinct functions along the hypoxia signaling pathways, such as malic acid, putrescine, xanthine oxidase-derived reactive oxygen species, and 2-oxoglutarate [32-35], but the majority of identified metabolites from this study have not been associated with the hypoxia pathway. Future study is warranted to elucidate their roles in cells under hypoxic stress.

Phosphoenolpyruvate carboxykinase (PEPCK), a key enzyme in the metabolic pathway of gluconeogenesis, converts oxaloacetate into phosphoen-olpyruvate [36]. PCK2, an isozyme of PEPCK, processes lactic acid that is continuously produced by red blood cells in the liver and kidney. PCK2 can regulate pancreatic neuroendocrine tumor cell proliferation by regulating glycolysis and mitochondrial oxidative phosphorylation, playing an important role in the adaptation of tumor cells to low glucose environments [37]. In tumor-repopulating cells of melanoma, PCK2 was down-regulated to promote the decomposition of citrate, which weakens the carbon flow in the tricarboxylic acid cycle, resulting in reduced oxidative phosphorylation [38]. PCK2 is frequently up-regulated in breast, colon, lung, prostate, thyroid, bladder,

Table 4. The correlation between clinical characteristics and expression of GLUT-1 and PCK2 in laryngeal squamous cell carcinoma tissues

Factor	*n*	GLUT-1		*P*	*r*	PCK2		*P*	*r*
		+	-			+	-		
Sex									
Male	42	36	6	0.653	0.062	36	6	0.238	0.164
Female	10	8	2			7	3		
Age									
≥ 60 years	25	22	3	0.515	0.900	23	2	0.088	0.237
< 60 years	27	22	5			20	7		
Tissue type									
High-middle differentiation	31	26	5	0.857	-0.250	25	6	0.635	-0.660
Poor differentiation	21	18	3			18	3		
Anatomical type									
Supraglottic and subglottic	25	21	4	0.906	-0.016	20	5	0.621	-0.068
Glottic	27	23	4			23	4		
Clinical stage									
I	19	13	6	0.014	0.341	12	7	0.005	0.392
II-IV	33	31	2			31	2		
Lymph node metastasis									
Yes	28	27	1	0.011	0.354	27	1	0.005	0.392
No	24	17	7			16	8		

Table 5. The correlation between GLUT-1 and PCK2 expression in laryngeal squamous cell carcinoma

GLUT-1	PCK2			
	+	-	*P*	*r*
+	39	5	0.007	0.368
-	4	4		

and kidney cancer cells [40-42]. However, the role of PCK2 in laryngeal cancer remains unclear.

In the current study, we have demonstrated that PCK2 is highly expressed in laryngeal cancer SCC10A cells and down-regulation of PCK2 inhibits the invasion and migration of laryngeal cancer cells, which are consistent with previous studies [29, 36, 43]. In the liver, there is the increased conversion of pyruvate to lactate in hypoxia, which can subsequently be converted to glucose by the gluconeogenesis, while the key enzyme of the pathway PCK2 was up-regulated in the liver [44], so the content of glucose and ATP increases with increased gluconeogenesis, which was consistent with the study that the glucose and ATP content in SCC10A cells were increased in hypoxia. PCK2 is in a unique position of cellular metabolism and plays a key role in the gluconeogenesis pathway by converting lactate to glucose in the liver [36, 44]. Down-regulation of PCK2 would weaken the gluconeogenesis pathway, leading to lactic acid accumulation and reduced glucose level, just as our data demonstrated.

We have shown that PCK2 is highly expressed in laryngeal squamous cell carcinoma and is positively associated with clinical stages and lymph node metastasis. GLUT-1 is also highly expressed in laryngeal squamous cell carcinoma, consistent with a previous report [45]. Interestingly, we demonstrated a positive correlation between the expression of GLUT-1 and PCK2. Given that GLUT-1 is a marker of hypoxia [24, 46], our results suggest that PCK2 may also be involved in the hypoxic pathway. However, the mechanisms of PCK2 in tumor hypoxia and laryngeal cancer tumorigenesis remain unclear and warrant further study.

In conclusion, our findings provided the evidence that down-regulation of PCK2 inhibits the invasion, migration, and proliferation of laryngeal cancer, suggesting that PCK2 plays an important role in tumorigenesis and pro-

gression of laryngeal cancer. In addition, the expression of PCK2 and GLUT-1 was positively correlated in laryngeal cancer. Given the critical role that tumor hypoxia plays in the prognosis of solid tumors, our data suggest PCK2 as a potential prognostic factor in laryngeal cancer patients. Taken together, our study provided evidence to suggest that targeting PCK2 may be a new therapeutic strategy for laryngeal cancer treatment.

Acknowledgements

This study was supported by the National Natural Science Foundation of China (no. 81272960), the Key Research Program from the Science and Technology Department of Hunan Province, China (no. 2017SK2082) and the Key Research Program from the Science and Technology Department of Ningxia Hui Autonomous Region, China (no. 2019BFH-02012), the Key Research Program of Hunan Health Committee (20201909) and the program of Hengyang science and Technology Bureau (2017-1, 2020-67).

Disclosure of conflict of interest

None.

Address correspondence to: Jianhong Zuo, Hengyang Medical School, University of South China, 28 Changsheng Road, Hengyang 421001, Hunan, P. R. China. E-mail: 632138414@qq.com

References

[1] Brandstorp-Boesen J, Falk RS, Boysen M and Brøndbo K. Long-term trends in gender, T-stage, subsite and treatment for laryngeal cancer at a single center. Eur Arch Otorhinolaryngol 2014; 271: 3233-3239.

[2] Liu Y, Zhao Q, Ding G, Zhu Y, Li W and Chen W. Incidence and mortality of laryngeal cancer in China, 2008-2012. Chin J Cancer Res 2018; 30: 580-587.

[3] Markou K, Christoforidou A, Karasmanis I, Tsiropoulos G, Triaridis S, Constantinidis I, Vital V and Nikolaou A. Laryngeal cancer: epidemiological data from Northern Greece and review of the literature. Hippokratia 2013; 17: 313-318.

[4] Wen X, Li ZF , Wang H, Sun SH, Guo X and Li FC. Effect of miR-200c regulation of Peptidyl-Prolyl Cis/Trans isomerase on the biological behavior of Hep-2 cells. J China Med Univ 2019; 48: 17-22.

[5] Jiang LY, Lian M, Wang H, Fang JG and Wang Q. Inhibitory effects of 5-Aza-2'-deoxycytidine and trichostatin A in combination with p53-expressing adenovirus on human laryngocarcinoma cells. Chin J Cancer Res 2012; 24: 232-237.

[6] Zuo J, Wen J, Lei M, Wen M, Li S, Lv X, Luo Z and Wen G. Hypoxia promotes the invasion and metastasis of laryngeal cancer cells via EMT. Med Oncol 2016; 33: 15.

[7] Mathieu J, Zhang Z, Zhou W, Wang AJ, Heddleston JM, Pinna CM, Hubaud A, Stadler B, Choi M, Bar M, Tewari M, Liu A, Vessella R, Rostomily R, Born D, Horwitz M, Ware C, Blau CA, Cleary MA, Rich JN and Ruohola-Baker H. HIF induces human embryonic stem cell markers in cancer cells. Cancer Res 2011; 71: 4640-4652.

[8] Pugh CW and Ratcliffe PJ. Regulation of angiogenesis by hypoxia: role of the HIF system. Nat Med 2003; 9: 677-684.

[9] Koh MY, Spivak-Kroizman TR and Powis G. HIF-1alpha and cancer therapy. Recent Results Cancer Res 2010; 180: 15-34.

[10] Huang X and Zuo J. Emerging roles of miR-210 and other non-coding RNAs in the hypoxic response. Acta Biochim Biophys Sin (Shanghai) 2014; 46: 220-232.

[11] Sceneay J, Chow MT, Chen A, Halse HM, Wong CS, Andrews DM, Sloan EK, Parker BS, Bowtell DD, Smyth MJ and Möller A. Primary tumor hypoxia recruits CD11b+/Ly6Cmed/Ly6G+ immune suppressor cells and compromises NK cell cytotoxicity in the premetastatic niche. Cancer Res 2012; 72: 3906-3911.

[12] Dziurla R, Gaber T, Fangradt M, Hahne M, Tripmacher R, Kolar P, Spies CM, Burmester GR and Buttgereit F. Effects of hypoxia and/or lack of glucose on cellular energy metabolism and cytokine production in stimulated human CD4+ T lymphocytes. Immunol Lett 2010; 131: 97-105.

[13] Mayer A and Vaupel P. Hypoxia, lactate accumulation, and acidosis: siblings or accomplices driving tumor progression and resistance to therapy? Adv Exp Med Biol 2013; 789: 203-209.

[14] Akram M. Mini-review on glycolysis and cancer. J Cancer Educ 2013; 28: 454-457.

[15] Birsoy K, Possemato R, Lorbeer FK, Bayraktar EC, Thiru P, Yucel B, Wang T, Chen WW, Clish CB and Sabatini DM. Metabolic determinants of cancer cell sensitivity to glucose limitation and biguanides. Nature 2014; 508: 108-112.

[16] Cioffi CL, Liu XQ, Kosinski PA, Garay M and Bowen BR. Differential regulation of HIF-1 alpha prolyl-4-hydroxylase genes by hypoxia in human cardiovascular cells. Biochem Biophys Res Commun 2003; 303: 947-953.

[17] Piret JP, Mottet D, Raes M and Michiels C. $CoCl_2$, a chemical inducer of hypoxia-inducible factor-1, and hypoxia reduce apoptotic cell death in hepatoma cell line HepG2. Ann N Y Acad Sci 2002; 973: 443-447.

[18] Chen R, Xu J, She Y, Jiang T, Zhou S, Shi H and Li C. Necrostatin-1 protects C2C12 myotubes from $CoCl_2$-induced hypoxia. Int J Mol Med 2018; 41: 2565-2572.

[19] Qiu Y, Cai G, Su M, Chen T, Zheng X, Xu Y, Ni Y, Zhao A, Xu LX, Cai S and Jia W. Serum metabolite profiling of human colorectal cancer using GC-TOFMS and UPLC-QTOFMS. J Proteome Res 2009; 8: 4844-4850.

[20] Wang JH, Chen WL, Li JM, Wu SF, Chen TL, Zhu YM, Zhang WN, Li Y, Qiu YP, Zhao AH, Mi JQ, Jin J, Wang YG, Ma QL, Huang H, Wu DP, Wang QR, Li Y, Yan XJ, Yan JS, Li JY, Wang S, Huang XJ, Wang BS, Jia W, Shen Y, Chen Z and Chen SJ. Prognostic significance of 2-hydroxyglutarate levels in acute myeloid leukemia in China. Proc Natl Acad Sci U S A 2013; 110: 17017-17022.

[21] Qiu Y, Cai G, Zhou B, Li D, Zhao A, Xie G, Li H, Cai S, Xie D, Huang C, Ge W, Zhou Z, Xu LX, Jia W, Zheng S, Yen Y and Jia W. A distinct metabolic signature of human colorectal cancer with prognostic potential. Clin Cancer Res 2014; 20: 2136-2146.

[22] Zuo JH, Ishikawa T, Boutros S, Xiao Z, Humtsoe JO and Kramer RH. Bcl-2 overexpression induces a partial epithelial to mesenchymal transition and promotes squamous carcinoma cell invasion and metastasis. Mol Cancer Res 2010; 8: 170-182.

[23] Zuo JH, Zhu W, Li MY, Li XH, Yi H, Zeng GQ, Wan XX, He QY, Li JH, Qu JQ, Chen Y and Xiao ZQ. Activation of EGFR promotes squamous carcinoma SCC10A cell migration and invasion via inducing EMT-like phenotype change and MMP-9-mediated degradation of E-cadherin. J Cell Biochem 2011; 112: 2508-2517.

[24] Zuo JH, Wen M, Lei M, Peng X, Yang X and Liu Z. MiR-210 links hypoxia with cell proliferation regulation in human Laryngocarcinoma cancer. J Cell Biochem 2015; 116: 1039-1049.

[25] Wang GL and Semenza GL. Desferrioxamine induces erythropoietin gene expression and hypoxia-inducible factor 1 DNA-binding activity: implications for models of hypoxia signal transduction. Blood 1993, 82: 3610-3615.

[26] Künzel J, Mantsopoulos K, Psychogios G, Agaimy A, Grundtner P, Koch M and Iro H. Lymph node ratio is of limited value for the decision-making process in the treatment of patients with laryngeal cancer. Eur Arch Otorhinolaryngol 2015; 272: 453-461.

[27] Haisfield-Wolfe ME, Brown C, Richardson M and Webster K. Variations in symptom severity patterns among oropharyngeal and laryngeal cancer outpatients during radiation treatment: a pilot study. Cancer Nurs 2015; 38: 279-287.

[28] Rinkel RN, Verdonck-de Leeuw IM, van den Brakel N, de Bree R, Eerenstein SE, Aaronson N and Leemans CR. Patient-reported symptom questionnaires in laryngeal cancer: voice, speech and swallowing. Oral Oncol 2014; 50: 759-764.

[29] Méndez-Lucas A, Hyroššová P, Novellasdemunt L, Viñals F and Perales JC. Mitochondrial phosphoenol-pyruvate carboxykinase (PEPCK-M) is a pro-survival, Endoplasmic Reticulum (ER) stress response gene Involved in tumor cell adaptation to nutrient availability. J Biol Chem 2014; 289: 22090-22102.

[30] Malm SW, Hanke NT, Gill A, Carbajal L and Baker AF. The anti-tumor efficacy of 2-deoxyglucose and D-allose are enhanced with p38 inhibition in pancreatic and ovarian cell lines. J Exp Clin Cancer Res 2015; 34: 31.

[31] Hakimi AA, Tickoo SK, Xu JN, Lee CH, Mano R, Chen YB, Stirdivant S, Neri B, Wolfert R, Fine SW, Al-Ahmadie H, Gopalan A, Russo P, Reuter VE and Hsieh JJ. Sorbitol as a novel mechanism of hypoxia-inducible factor (HIF) pathway activation in clear cell papillary renal cell carcinoma (CCPRCC). J Urol 2014; 191: e377-e378.

[32] Tang X, Liu J, Dong W, Li P, Li L, Lin C, Zheng Y, Hou J and Li D. The cardioprotective effects of citric Acid and L-malic Acid on myocardial ischemia/reperfusion injury. Evid Based Complementary Alternat Med 2013; 2013: 820695.

[33] Ruchko M, Gillespie MN, Weeks RS, Olson JW and Babal P. Putrescine transport in hypoxic rat main PASMCs is required for p38 MAP kinase activation. Am J Physiol Lung Cell Mol Physiol 2003; 284: L179-L186.

[34] Griguer CE, Oliva CR, Kelley EE, Giles GI, Lancester JR and Gillespie GY. Xanthine oxidase-dependent regulation of hypoxia-inducible factor in cancer cells. Cancer Res 2006; 66: 2257-2263.

[35] Kaelin WG Jr. Cancer and altered metabolism: potential importance of hypoxia- inducible factor and 2-oxoglutarate-dependent dioxygenases. Cold Spring Harb Symp Quant Biol 2011; 76: 335-345.

[36] Leithner K. PEPCK in cancer cell starvation. Oncoscience 2015; 2: 805-806.

[37] Chu PY, Jiang SS, Shan YS, Hung WC, Chen MH, Lin HY, Chen YL, Tsai HJ and Chen LT. Mitochondrial phosphoenolpyruvate carboxykinase (PEPCK-M) regulates the cell metabolism of pancreatic neuroendocrine tumors (pNET) and de-sensitizes pNET to mTOR inhibitors. Oncotarget 2017; 8: 103613-103625.

[38] Luo S, Li Y, Ma R, Liu J, Xu P, Zhang H, Tang K, Ma J, Liu N, Zhang Y, Sun Y, Ji T, Liang X, Yin X, Liu Y, Tong W, Niu Y, Wang N, Wang X and Huang B. Downregulation of PCK2 remodels tricarboxylic acid cycle in tumor-repopulating cells of melanoma. Oncogene 2017; 36: 3609-3617.

[39] Leithner K, Hrzenjak A, Trőtzmüller, M, Moustafa T, Köfeler HC, Wohlkoenig C, Stacher E, Lindenmann J, Harris AL, Olschewski A and Olschewski H. PCK2 activation mediates an adaptive response to glucose depletion in lung cancer. Oncogene 2015; 34: 1044-1050.

[40] Montal ED, Dewi R, Bhalla K, Ou L, Hwang BJ, Ropell AE, Gordon C, Liu WJ, DeBerardinis RJ, Sudderth J, Twaddel W, Boros LG, Shroyer KR, Duraisamy S, Drapkin R, Powers RS, Rohde JM, Boxer MB, Wong KK and Girnun GD. PEPCK coordinates the regulation of central carbon metabolism to promote cancer cell growth. Mol Cell 2015; 60: 571- 583.

[41] Zhao J, Li J, Fan TWM and Hou SX. Glycolytic reprogramming through PCK2 regulates tumor initiation of prostate cancer cells. Oncotarget 2017; 8: 83602-83618.

[42] Vincent EE, Sergushichev A, Griss T, Gingras MC, Samborska B, Ntimbane T, Coelho PP, Blagih J, Raissi TC, Choinière L, Bridon G, Loginicheva E, Flynn BR, Thomas EC, Tavaré JM, Avizonis D, Pause A, Elder DJ, Artyomov MN and Jones RG. Mitochondrial phosphoenolpyruvate carboxykinase regulates metabolic adaptation and enables glucose-independent tumor growth. Mol Cell 2015; 60: 195-207.

[43] Balsa-martinez E and Puigserver P. Cancer cells hijack gluconeogenic enzymes to fuel cell growth. Mol Cell 2015; 60: 509-511.

[44] Willems E, Hu TT, Soler Vasco L, Buyse J, Decuypere E, Arckens L and Everaert N. Embryonic protein undernutrition by albumen removal programs the hepatic amino acid and glucose metabolism during the perinatal period in an avian model. PLoS One 2014; 9: e94902.

[45] Abdou AG, Eldien MM and Elsakka D. GLUT-1 expression in cutaneous basal and squamous cell carcinomas. Int J Surg Pathol 2015; 23: 447-453.

[46] Blayney JK, Cairns L, Li G, McCabe N, Stevenson L, Peters CJ, Reid NB, Spence VJ, Chisambo C, McManus D, James J, McQuaid S, Craig S, Arthur K, McArt D, Ong CJ, Lao-Sirieix P, Hamilton P, Salto-Tellez M, Eatock M, Coleman HG, Fitzgerald RC, Kennedy RD and Turkington RC; Oesophageal Cancer Clinical and Molecular Stratification (OCCAMS) Study Group. Glucose transporter 1 expression as a marker of prognosis in oesophageal adenocarcinoma. Oncotarget 2018; 9: 18518-18528.

Supplementary Table 1. Identity and quantification of the 155 differentially expressed proteins consistently identified in all three experiments

Protein accession	Gene name	Regulated type	*P* value	MW [kDa]	Score	Coverage [%]	Peptides	Experiment 1		Experiment 2		Experiment 3	
								hypoxia	normoxia	hypoxia	normoxia	hypoxia	normoxia
O00461	GOLIM4	Down	0.0000621	81.879	66.781	17	11	0.554	0.959	0.596	0.993	0.585	0.929
O43653	PSCA	Down	0.0000808	12.912	36.234	14.6	2	0.296	0.786	0.311	0.732	0.334	0.688
O60353	FZD6	Down	0.0142	79.291	4.6638	2.7	2	0.463	0.703	0.458	0.83	0.603	0.869
O60503	ADCY9	Down	0.0181	150.7	1.9491	1	1	0.681	1.003	0.666	1.081	0.507	0.846
O60635	TSPAN1	Down	0.0000182	26.301	16.973	5.4	1	0.309	0.804	0.323	0.882	0.29	0.842
O95081	AGFG2	Down	0.0018	48.962	13.45	10.4	4	0.666	1.124	0.55	1.177	0.711	1.123
O95084	PRSS23	Down	0.021	43.001	3.9359	5.5	2	0.557	0.905	0.291	0.919	0.45	0.783
P02795	MT2A	Down	0.00472	6.0422	20.837	67.2	4	0.726	1.517	1.009	1.465	0.764	1.706
P0DJ93	SMIM13	Down	0.0234	10.351	3.7846	13.2	2	0.707	1.009	0.675	1.18	0.882	1.433
P15954	COX7C	Down	0.0102	7.2454	5.97	28.6	2	0.401	1.082	0.511	1.098	0.519	1.067
P19971	TYMP	Down	0.0242	49.955	2.9507	2.3	1	0.509	1.057	0.763	0.952	0.632	0.914
P30613	PKLR	Down	0.0000822	61.829	1.768	3.3	2	0.747	1.476	0.667	1.45	0.639	1.494
P30626	SRI	Down	0.00000186	21.676	60.056	55.1	10	0.845	1.269	0.863	1.26	0.837	1.29
P35354	PTGS2	Down	0.000659	68.995	28.796	17.1	10	0.797	1.332	0.743	1.174	0.816	1.333
P37268	FDFT1	Down	0.0000353	48.115	69.968	24.7	9	0.623	0.964	0.646	0.969	0.625	0.922
P41221	WNT5A	Down	0.0103	42.339	6.5561	5.5	2	0.362	0.83	0.324	0.692	0.513	0.852
P50238	CRIP1	Down	0.000215	8.5328	4.1296	31.2	3	0.691	1.111	0.745	1.088	0.71	1.029
P53384	NUBP1	Down	0.0022	34.534	12.688	9.1	2	0.762	1.454	0.781	1.631	0.801	1.219
P79522	PRR3	Down	0.00574	20.64	1.7832	11.7	2	0.742	0.988	0.777	1.259	0.749	1.227
Q02487	DSC2	Down	0.0402	99.961	2.7101	2.6	2	0.25	0.797	0.147	0.835	0.35	0.766
Q02818	NUCB1	Down	0.000322	53.879	116.61	39.9	15	0.715	1.151	0.737	1.031	0.706	1.062
Q04828	AKR1C1	Down	0.000605	36.788	49.711	29.1	8	0.795	1.215	0.862	1.39	0.81	1.36
Q08AF3	SLFN5	Down	0.00952	101.05	14.491	9	8	0.873	1.093	0.671	1.084	0.715	1.227
Q11206	ST3GAL4	Down	0.00198	38.045	1.5879	2.4	1	0.668	1.039	0.672	0.888	0.627	1.039
Q13332	PTPRS	Down	0.00336	217.04	11.228	2.5	5	0.498	1.206	0.4	1.063	0.618	1.112
Q15070	OXA1L	Down	0.0142	48.547	10.629	12.2	6	0.659	0.945	0.563	0.937	0.649	0.961
Q15818	NPTX1	Down	0.000344	47.122	2.2993	3.9	2	0.582	1.253	0.571	1.399	0.464	1.303
Q16850	CYP51A1	Down	0.000317	56.805	37.196	17.7	8	0.616	1.12	0.698	1.082	0.69	1.16
Q2TAA8	TSNAXIP1	Down	0.00136	76.772	1.1557	1.1	1	0.625	1.025	0.652	1.043	0.711	0.931
Q5U649	C12orf60	Down	0.0484	27.626	1.9216	3.3	1	0.565	1.042	0.463	0.787	0.732	0.869
Q6ZRQ5	MMS22L	Down	0.00902	142.32	8.401	2.1	3	0.728	0.9	0.545	1.009	0.621	1.034
Q86UY6	NAA40	Down	0.00986	27.194	3.1982	5.1	1	0.583	0.992	0.773	1.138	0.603	1.334
Q8N697	SLC15A4	Down	0.0468	62.033	2.0451	2.4	1	0.553	0.802	0.513	1.412		1.35

Q92896	GLG1	Down	0.0000643	134.55	37.42	15.1	17	0.677	1.221	0.674	1.211	0.738	1.173
Q96J42	TXNDC15	Down	0.0153	39.885	6.6127	8.6	2	0.626	1.025	0.873	1.219	0.662	1.219
Q99439	CNN2	Down	0.00178	33.697	30.196	24.6	7	0.642	1.167	0.772	1.099	0.665	1.055
Q99643	SDHC	Down	0.002	18.61	5.215	12.4	2	0.627	1.039	0.613	1.006	0.606	0.852
Q9BPX6	MICU1	Down	0.000478	54.351	9.7659	6.5	2	0.418	1.155	0.325	1.21	0.295	1.03
Q9BRK5	SDF4	Down	0.0143	41.806	90.709	16.6	5	0.663	1.087	0.589	1.083	0.722	1.055
Q9BS40	LXN	Down	0.000724	25.75	6.2676	8.6	2	0.938	1.44	0.921	1.572	0.95	1.342
Q9BT40	INPP5K	Down	0.001	51.09	3.4122	2.2	1	0.593	0.955	0.61	1.018	0.674	0.913
Q9BWS9	CHID1	Down	0.00404	44.94	3.174	5.1	2	0.537	1.254	0.531	1.214	0.733	1.075
Q9H3M7	TXNIP	Down	0.000204	43.661	6.8382	10.5	3	0.601	1.259	0.621	1.125	0.658	1.11
Q9NRY2	INIP	Down	0.0332	11.425	5.2368	12.5	1	0.775	1.041	0.422	1.232	0.727	1.338
Q9NX02	NDUFA4	Down	0.0128	9.032	3.629	7.6	2	0.78	1.121	0.493	1.175	0.674	1.039
Q9NX14	NDUFB11	Down	0.0059	17.316	17.746	33.3	3	0.633	1.072	0.558	0.89	0.692	0.962
Q9NZ08	ERAP1	Down	0.0156	107.23	4.0061	5	4	0.89	1.11	0.671	1.246	0.671	1.578
Q9NZP5	OR5AC2	Down	0.000676	35.304	1.197	2.3	1	0.467	0.926	0.515	0.904	0.573	0.959
Q9UII2	ATPIF1	Down	0.000524	12.249	8.7239	17	4	0.254	1.503	0.271	1.383	0.412	1.489
Q9Y5K1	SPO11	Down	0.00144	44.536	-2	1.8	1	0.588	0.993	0.468	0.902	0.487	0.909
Q9Y6N7	ROBO1	Down	0.0000231	180.93	4.2666	2.8	4	0.74	1.207	0.688	1.18	0.693	1.2
A6NLE4	SMIM23	Up	0.0000601	20.025	-2	5.2	1	1.45	0.434	1.569	0.361	1.668	0.44
O00622	CYR61	Up	0.000255	42.026	39.825	21.3	8	1.44	0.766	1.455	0.835	1.567	0.711
O14503	BHLHE40	Up	0.00044	45.51	1.7773	1.9	1	1.545	0.864	1.61	0.953	1.624	1.015
O14879	IFIT3	Up	0.0367	55.984	19.669	10.4	4	1.525	0.847	1.755	0.562	0.965	0.729
O60292	SIPA1L3	Up	0.0102	194.61	3.7659	1.3	2	1.153	0.718	1.417	0.735	1.349	0.946
O75190	DNAJB6	Up	0.002	36.087	32.477	19.6	6	1.256	0.814	1.502	0.807	1.34	0.673
O75446	SAP30	Up	0.0242	23.306	7.6145	13.6	3	1.635	0.929	1.872	0.545	1.3	0.367
O75496	GMNN	Up	0.000324	23.565	2.3927	4.3	1	1.468	0.915	1.509	0.954	1.37	0.989
O76061	STC2	Up	0.000342	33.248	5.0592	7	2	1.796	0.502	1.636	0.496	1.692	0.353
O76080	ZFAND5	Up	0.000000211	23.132	2.6616	4.2	1	2.195	0.435	2.146	0.422	2.243	0.401
O95391	SLU7	Up	0.000444	68.386	10.303	9.6	6	1.244	0.826	1.222	0.736	1.178	0.818
O95817	BAG3	Up	0.000136	61.594	103.31	29	15	1.646	0.751	1.685	0.822	1.478	0.754
P01100	FOS	Up	0.0118	40.695	9.6284	6.8	2	1.915	0.677	1.647	0.359	1.852	0.828
P01106	MYC	Up	0.00166	48.804	4.2537	4.6	2	1.377	0.691	1.167	0.691	1.578	0.721
P04792	HSPB1	Up	0.000124	22.782	99.873	47.8	10	1.4	0.941	1.412	0.903	1.517	0.951
P05412	JUN	Up	0.000718	35.675	8.0631	13	3	1.748	0.752	1.682	0.649	1.826	0.523
P05423	POLR3D	Up	0.000818	44.395	5.9117	5.8	2	1.292	0.787	1.361	0.908	1.254	0.84

P08243	ASNS	Up	0.000316	64.369	55.307	28	15	1.542	0.944	1.584	0.9	1.39	0.913
P09601	HMOX1	Up	0.00336	32.818	30.231	31.9	8	1.879	0.562	1.82	0.464	1.864	0.434
P0DMV9	HSPA1B	Up	0.00000068	70.051	314.36	49.9	29	1.995	0.598	1.885	0.566	1.948	0.604
P15036	ETS2	Up	0.00154	53.001	2.1085	1.9	1	1.348	0.898	1.331	0.767	1.412	0.921
P15408	FOSL2	Up	0.000000979	35.193	3.4581	6.1	2	1.282	0.807	1.291	0.805	1.308	0.829
P17066	HSPA6	Up	0.001	71.027	14.332	24.1	13	1.474	0.721	1.518	0.74	1.215	0.652
P17275	JUNB	Up	0.000278	35.879	45.181	22.5	5	1.365	0.885	1.452	0.843	1.466	0.943
P18847	ATF3	Up	0.000017	20.575	1.829	4.4	1	1.938	0.449	2.014	0.462	1.85	0.389
P20908	COL5A1	Up	0.0000635	183.56	34.782	7.4	13	1.511	0.813	1.488	0.758	1.373	0.784
P22736	NR4A1	Up	0.00106	64.463	8.8124	9.7	5	1.449	0.817	1.203	0.763	1.401	0.73
P25685	DNAJB1	Up	0.0000165	38.044	80.977	43.5	14	1.605	0.722	1.703	0.729	1.702	0.67
P31689	DNAJA1	Up	0.00000313	44.868	84.66	32	11	1.516	0.813	1.471	0.764	1.481	0.779
P35222	CTNNB1	Up	0.00596	85.496	24.506	10.9	7	1.293	0.655	1.307	0.758	1.141	0.872
P35625	TIMP3	Up	0.00124	24.145	6.1432	15.6	3	1.281	0.752	1.211	0.727	1.359	0.604
P35790	CHKA	Up	0.000658	52.248	2.6411	2	1	1.41	0.855	1.403	0.837	1.303	0.731
P41273	TNFSF9	Up	0.000116	26.624	5.0989	10.6	2	1.397	0.667	1.419	0.682	1.271	0.609
P42684	ABL2	Up	0.00000365	128.34	4.0112	1.4	1	1.461	0.755	1.546	0.742	1.452	0.725
P48507	GCLM	Up	0.000137	30.727	115.91	28.5	6	1.505	0.913	1.5	0.996	1.443	0.98
P49759	CLK1	Up	0.0000951	57.29	15.727	10.1	5	1.651	0.675	1.616	0.57	1.712	0.679
P51784	USP11	Up	0.00194	109.82	20.829	5.8	5	1.375	0.762	1.201	0.674	1.606	0.715
P52789	HK2	Up	0.000823	102.38	144.48	25.4	21	1.55	0.992	1.36	0.943	1.557	0.981
P61927	RPL37	Up	0.000539	11.078	1.1521	16.5	2	1.446	0.737	1.311	0.836	1.286	0.738
P62699	YPEL5	Up	0.0437	13.841	4.0237	19.8	2	1.281	0.786	1.247	0.716	1.286	0.983
P63146	UBE2B	Up	0.000717	17.312	2.2638	11.2	1	1.464	1.017	1.578	0.938	1.474	0.874
Q01581	HMGCS1	Up	0.0016	57.293	14.027	10.8	6	1.52	0.754	1.399	0.931	1.467	0.901
Q12983	BNIP3	Up	0.000295	27.832	3.2158	9.3	3	2.039	0.586	1.928	0.587	2.063	0.582
Q13501	SQSTM1	Up	0.0109	47.687	141.51	42.7	10	1.44	0.788	1.437	0.834	1.472	0.666
Q13751	LAMB3	Up	0.0113	129.57	4.3796	3	3	1.154	0.747	1.347	0.835	1.2	0.565
Q14978	NOLC1	Up	0.00538	73.602	28.128	17	13	1.369	0.867	1.259	0.858	1.4	0.864
Q15011	HERPUD1	Up	0.0000157	43.719	4.3589	4.3	2	1.667	0.592	1.601	0.646	1.58	0.653
Q15014	MORF4L2	Up	0.0000176	32.307	31.049	25.7	7	1.465	0.736	1.387	0.696	1.479	0.738
Q15047	SETDB1	Up	0.00002	143.16	1.7358	1.2	3	2.258	0.342	1.874	0.3	1.953	0.281
Q15276	RABEP1	Up	0.000122	99.289	12.798	5.6	5	1.808	0.594	1.96	0.728	1.729	0.665
Q15545	TAF7	Up	0.0047	40.259	9.9128	12.3	4	1.399	0.792	1.118	0.754	1.473	0.835
Q15742	NAB2	Up	0.0059	56.593	2.5618	2.1	1	1.251	0.791	1.523	0.725	1.452	0.956
Q16649	NFIL3	Up	0.000523	51.471	11.979	8.4	3	1.217	0.751	1.392	0.72	1.253	0.804

Q16665	HIF1A	Up	0.00208	92.669	13.43	3.4	3	2.299	0.407	2.26	0.32	2.303	0.412
Q16822	PCK2	Up	0.0000171	70.698	70.517	26.1	14	1.225	0.802	1.201	0.778	1.188	0.763
Q16875	PFKFB3	Up	0.00384	59.608	7.3249	7.3	4	1.463	0.464	1.793	0.691	2.001	0.738
Q16877	PFKFB4	Up	0.0018	54.039	6.3186	7.5	3	1.654	0.894	1.778	0.813	1.627	1.061
Q309B1	TRIM16L	Up	0.00292	40.305	13.021	5.7	1	1.367	0.711	1.268	0.797	1.45	0.911
Q504T8	MIDN	Up	0.0000382	49.212	1.8911	6.8	2	1.852	0.502	1.766	0.593	1.891	0.493
Q53GA4	PHLDA2	Up	0.00228	17.092	2.6162	5.9	1	1.498	0.715	1.572	0.884	1.33	0.866
Q5BKY9	FAM133B	Up	0.0043	28.385	4.364	7.3	2	1.221	0.735	1.135	0.848	1.113	0.668
Q5NDL2	EOGT	Up	0.00202	62.01	1.6111	3	2	2.084	0.209	1.928	0.467	1.613	0.34
Q5U3C3	TMEM164	Up	0.0000814	33.507	3.7111	8.4	2	1.197	0.494	1.204	0.501	1.417	0.47
Q5VY09	IER5	Up	0.0305	33.703	2.5743	5.2	1	2.353	0.384	2.506	0.404	2.125	0.125
Q6NYC1	JMJD6	Up	0.000517	46.461	4.4433	3.2	1	1.884	0.861	1.694	0.798	1.838	0.988
Q6UW68	TMEM205	Up	0.000603	21.198	7.8345	15.9	2	0.996	0.666	1.142	0.692	1.085	0.715
Q6ZW31	SYDE1	Up	0.000316	79.792	9.9729	6.5	5	1.498	0.83	1.526	0.947	1.43	0.91
Q6ZW76	ANKS3	Up	0.000762	72.037	1.7992	1.4	1	1.279	0.907	1.435	0.851	1.446	0.806
Q719H9	KCTD1	Up	0.0374	29.404	1.7383	5.4	1	1.127	0.9	1.376	0.823	1.296	0.521
Q86V24	ADIPOR2	Up	0.0000447	43.883	1.6836	3.1	1	1.526	0.612	1.733	0.652	1.63	0.572
Q86VP1	TAX1BP1	Up	0.0299	90.876	5.8086	5.6	5	1.257	0.805	1.181	0.946	1.15	0.608
Q8IUC4	RHPN2	Up	0.000198	76.992	6.1243	3.6	3	1.585	0.93	1.502	0.827	1.462	0.852
Q8IWT1	SCN4B	Up	0.00612	24.969	1.2347	3.9	1	1.455	0.79	1.438	0.986	1.297	0.724
Q8N9N8	EIF1AD	Up	0.000698	19.053	18.092	28.5	3	1.489	0.716	1.544	0.821	1.342	0.837
Q8NDZ4	C3orf58	Up	0.0012	49.481	2.6295	4.7	2	1.277	0.895	1.378	0.789	1.235	0.878
Q8TAD8	SNIP1	Up	0.0387	45.777	16.326	13.6	4	1.62	0.78	1.068	0.709	1.105	0.891
Q92598	HSPH1	Up	0.000101	96.864	187.3	43.1	31	1.667	0.908	1.591	0.864	1.492	0.914
Q96C19	EFHD2	Up	0.000381	26.697	30.667	20.4	5	1.529	0.961	1.354	0.91	1.42	0.919
Q96EB6	SIRT1	Up	0.00106	81.68	13.921	7.9	5	1.343	0.853	1.562	0.812	1.633	0.904
Q96IJ6	GMPPA	Up	0.000796	46.291	9.3117	8.8	3	1.546	0.459	1.371		1.612	0.525
Q99741	CDC6	Up	0.00894	62.72	9.7519	9.8	4	1.392	0.58	1.266	0.711	1.421	0.905
Q99828	CIB1	Up	0.0168	21.703	7.1311	22	4	1.544	1.083	1.374	0.775	1.292	0.881
Q99878	HIST1H2AJ	Up	0.00102	13.936	7.5906	26.6	4	1.315	0.727	1.266	0.818	1.461	0.839
Q9BT73	PSMG3	Up	0.00272	13.104	8.5265	10.7	1	1.552	0.876	1.354	0.921	1.272	0.948
Q9BY42	RTFDC1	Up	0.0000206	33.886	32.484	29.1	7	1.256	0.803	1.3	0.816	1.236	0.78
Q9BZQ8	FAM129A	Up	0.000241	103.13	10.659	5.3	4	1.447	0.786	1.308	0.8	1.538	0.779
Q9GZQ8	MAP1LC3B	Up	0.00306	14.688	9.3815	11.2	1	1.801	0.673	1.843	0.678	1.564	0.69
Q9H1E3	NUCKS1	Up	0.000959	27.296	69.705	15.6	3	1.602	0.91	1.474	0.782	1.481	0.942
Q9H270	VPS11	Up	0.0168	107.84	5.3096	3.9	3	1.024	0.694	0.999	0.467	1.081	0.695

Q9H3C7	GGNBP2	Up	0.00428	79.086	3.5141	1.9	1	1.527	0.533	1.511	0.853	1.875	0.647
Q9H6Z9	EGLN3	Up	0.00044	27.261	8.2736	5	1	2.307	0.417	2.023	0.579	1.99	0.615
Q9NNX1	TUFT1	Up	0.000223	44.263	4.4102	6.7	3	1.286	0.816	1.313	0.729	1.335	0.822
Q9NP50	SINHCAF	Up	0.0000613	24.852	2.4688	4.1	1	1.224	0.676	1.347	0.631	1.223	0.652
Q9NQ92	COPRS	Up	0.000384	20.066	9.5013	10.9	2	1.571	0.967	1.595	1.028	1.433	0.957
Q9NS87	KIF15	Up	0.0455	160.16	4.9435	2.7	4	1.747	0.649	1.463	0.623	1.124	1.081
Q9NUL7	DDX28	Up	0.0275	59.58	2.422	3.3	2	1.098	0.736	1.014	0.532	0.803	0.535
Q9P209	CEP72	Up	0.0382	71.717	5.2095	1.5	1	1.586	0.561	1.128	0.987	1.359	0.768
Q9UBU8	MORF4L1	Up	0.000261	41.473	18.231	18.2	6	1.864	0.465	1.854	0.499	1.859	0.47
Q9UBZ4	APEX2	Up	0.0011	57.4	14.775	8.7	3	1.31	0.842	1.201	0.843	1.419	0.776
Q9UDY4	DNAJB4	Up	0.00000424	37.806	58.597	31.5	8	1.793	0.712	1.809	0.7	1.656	0.732
Q9UJY1	HSPB8	Up	0.006	21.604	1.6927	9.2	2	1.454	0.88	1.231	0.876	1.253	0.71
Q9ULV3	CIZ1	Up	0.00796	100.04	8.0893	3.6	2	1.91	0.288	1.421	0.298	2.495	0.676
Q9ULX6	AKAP8L	Up	0.0244	71.648	9.6274	5.9	3	1.376	0.894	1.347	0.761	1.784	1.103
Q9Y244	POMP	Up	0.00306	15.789	3.4202	14.9	2	1.645	0.974	1.519	1.085	1.459	0.875
Q9Y605	MRFAP1	Up	0.0168	14.649	5.4262	14.2	2	1.279	1.047	1.493	0.688	1.662	0.728

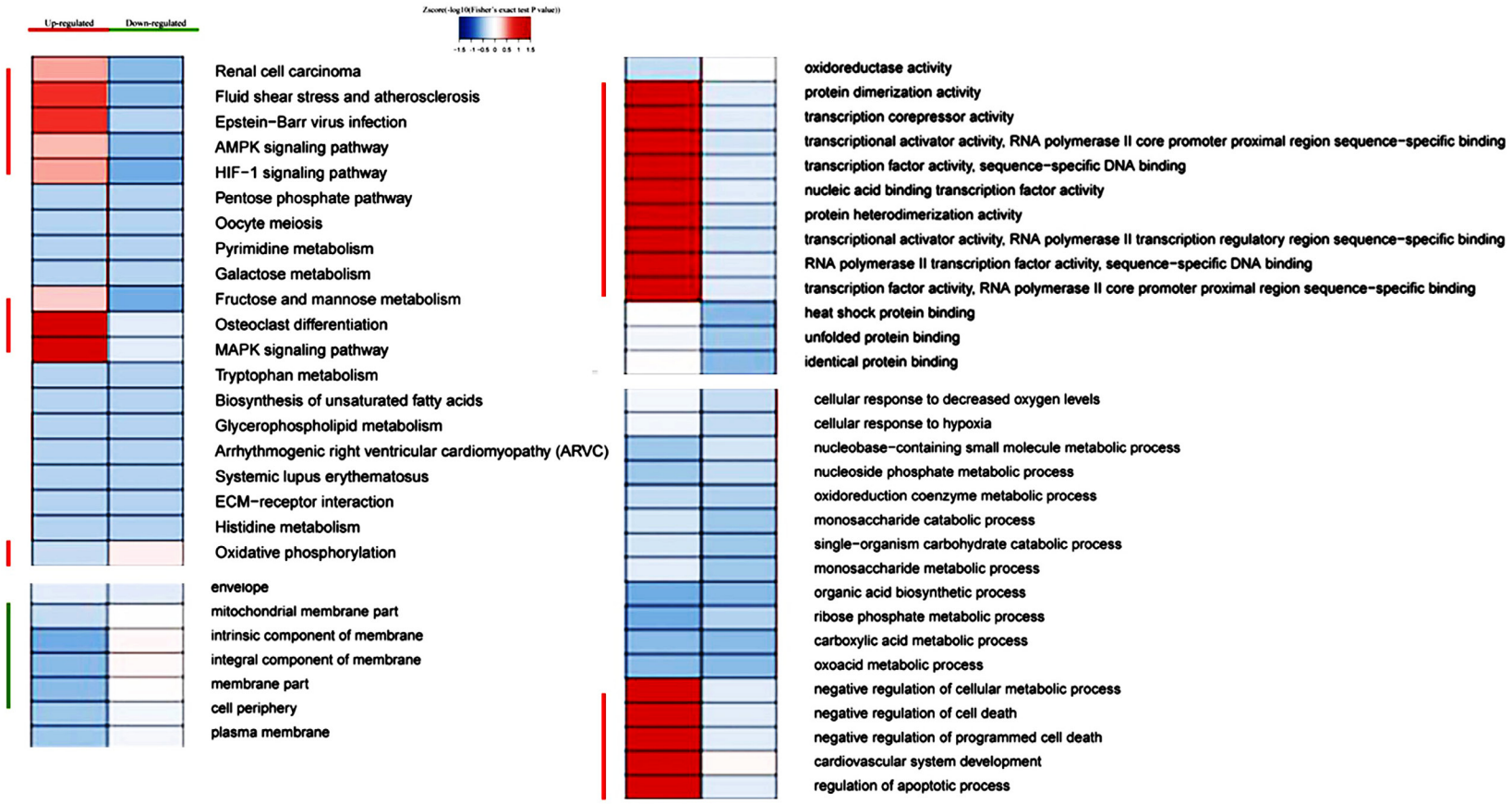

Supplementary Figure 1. Hierarchical clustering of the pathways the 155 differentially expressed proteins represent. The pathways enriched among the upregulated and downregulated proteins when the SCC10A cells were cultured with $CoCl_2$ were marked with red and green bars, respectively.

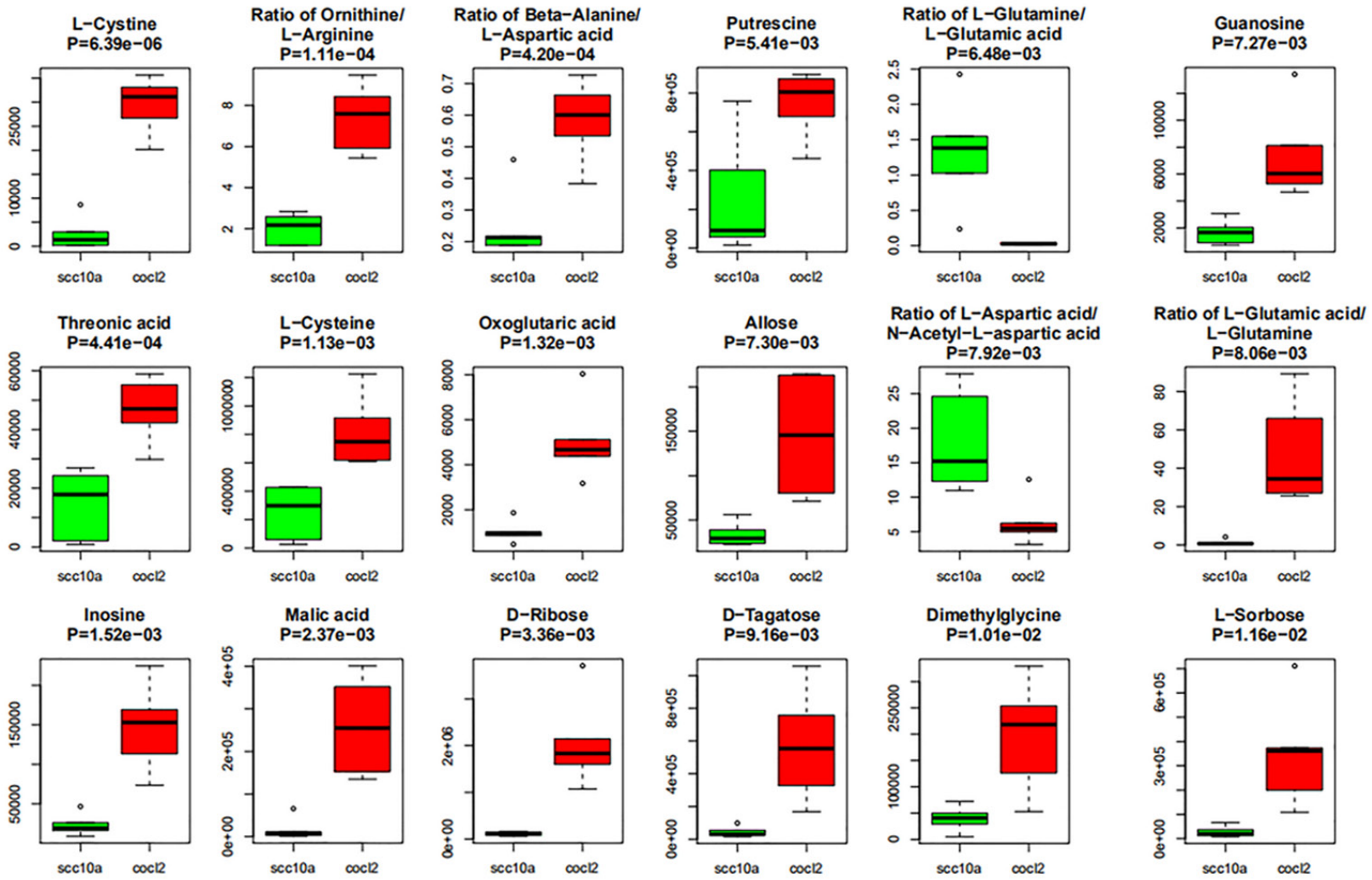
L−Cystine
P=6.39e−06
Ratio of Ornithine/
L−Arginine
P=1.11e−04
Ratio of Beta−Alanine/
L−Aspartic acid
P=4.20e−04
Putrescine
P=5.41e−03
Ratio of L−Glutamine/
L−Glutamic acid
P=6.48e−03
Guanosine
P=7.27e−03
Threonic acid
P=4.41e−04
L−Cysteine
P=1.13e−03
Oxoglutaric acid
P=1.32e−03
Allose
P=7.30e−03
Ratio of L−Aspartic acid/
N−Acetyl−L−aspartic acid
P=7.92e−03
Ratio of L−Glutamic acid/
L−Glutamine
P=8.06e−03
Inosine
P=1.52e−03
Malic acid
P=2.37e−03
D−Ribose
P=3.36e−03
D−Tagatose
P=9.16e−03
Dimethylglycine
P=1.01e−02
L−Sorbose
P=1.16e−02
scc10a
cocl2

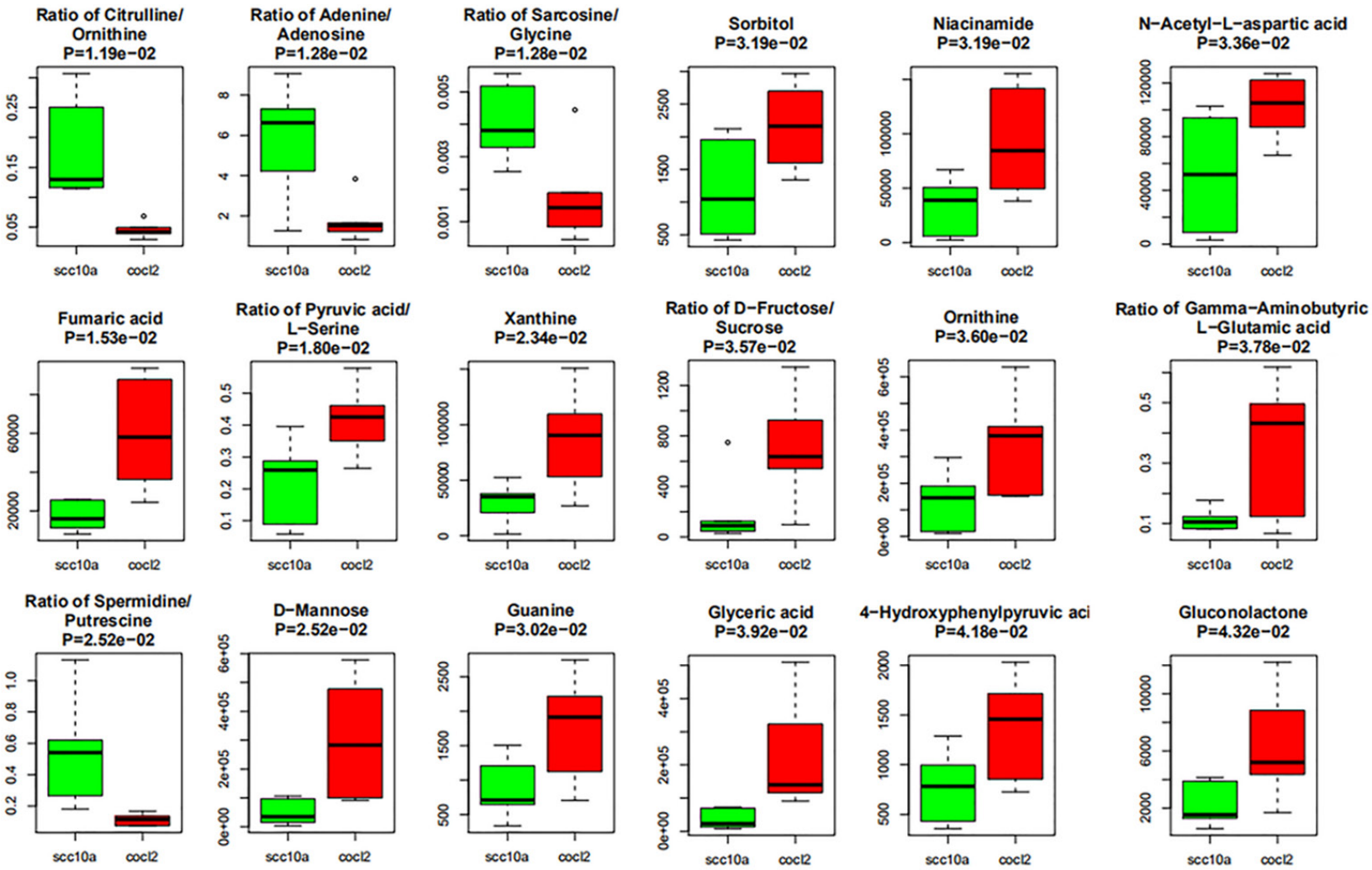
Ratio of Citrulline/ Ornithine P=1.19e-02
Ratio of Adenine/ Adenosine P=1.28e-02
Ratio of Sarcosine/ Glycine P=1.28e-02
Sorbitol P=3.19e-02
Niacinamide P=3.19e-02
N-Acetyl-L-aspartic acid P=3.36e-02
Fumaric acid P=1.53e-02
Ratio of Pyruvic acid/ L-Serine P=1.80e-02
Xanthine P=2.34e-02
Ratio of D-Fructose/ Sucrose P=3.57e-02
Ornithine P=3.60e-02
Ratio of Gamma-Aminobutyric L-Glutamic acid P=3.78e-02
Ratio of Spermidine/ Putrescine P=2.52e-02
D-Mannose P=2.52e-02
Guanine P=3.02e-02
Glyceric acid P=3.92e-02
4-Hydroxyphenylpyruvic aci P=4.18e-02
Gluconolactone P=4.32e-02
scc10a
cocl2

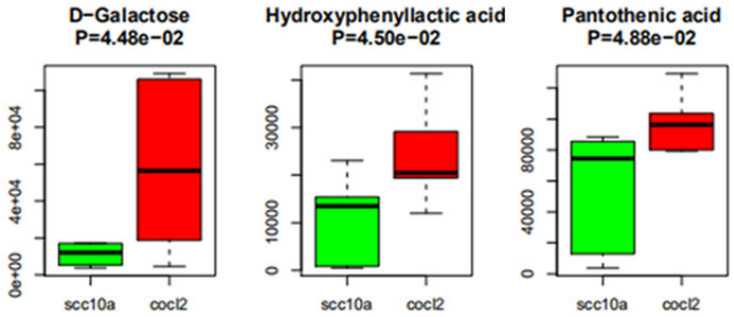

Supplementary Figure 2. Top ranked differentially produced metabolites in the cells cultured with or without $CoCl_2$.

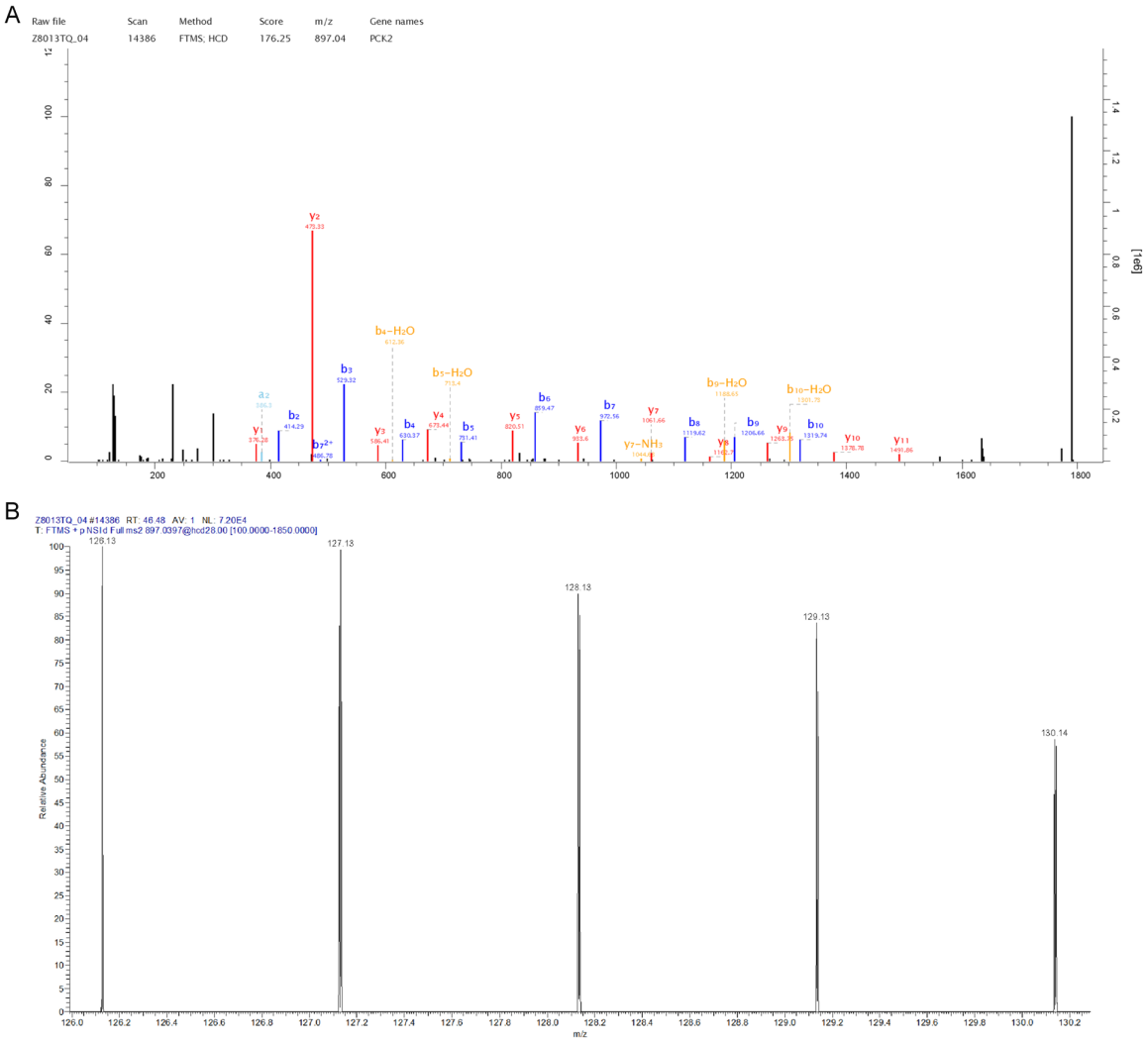

Supplementary Figure 3. LC-MS/MS spectra used for the identification and quantitation of PCK2. A. the sequence of AIDTTQLFSLPK allows the identification of PCK2 according to the matched peaks is shown. B. the released iTRAQ reporter ions provide relative quantitation of PCK2 from the SCC10A cells evaluated.